View Article Online
View Journal

Dalton Transactions

An international journal of inorganic chemistry

Accepted Manuscript

This article can be cited before page numbers have been issued, to do this please use: Y. Huentupil, P. Chung, N. A. Novoa, R. Arancibia, P. Roussel, J. Oyarzo, A. H. Klahn, C. Silva, C. Calvis, R. Messeguer, B. Ramon and C. López, *Dalton Trans.*, 2020, DOI: 10.1039/D0DT01756F.

ROYAL SOCIETY OF CHEMISTRY

rsc.li/dalton

View Article Online
DOI: 10.1039/D0DT01756F

ARTICLE

Novel Homo- (Fe_2) and Heterobimetallic [(Fe,M) with M = Re or Mn] Sulfonyl Hydrazones

Received 00th January 20xx,
Accepted 00th January 20xx

DOI: 10.1039/x0xx00000x

Yosselin Huentupil,[a] Patricio Chung,[a] Néstor Novoa,[a] Rodrigo Arancibia,*[a] Pascal Roussel,[b] Juan Oyarzo,[c] A. Hugo Klahn,[c] Carlos P. Silva,[d] Carme Calvis,[e] Ramon Messeguer,[e] Ramón Bosque,[f] Concepción López *[f]

Abstract. The synthesis and characterization of the novel ferrocenyl sulfonyl hydrazide [Fe(η^5-C_5H_5){(η^5-C_5H_4)-S(O)$_2$-NH-NH_2}] (**2**) is reported. Additional studies on its reactivity in front of acetone or the ferrocenyl-, cyrhetrenyl- or cymantrenyl-aldehydes have allowed us to isolate and characterize: [Fe(η^5-C_5H_5){(η^5-C_5H_4)-S(O)$_2$-NH-N=CMe$_2$}] (**3**), the bis(ferrocenyl) derivative: [Fe(η^5-C_5H_5){[(η^5-C_5H_4)-S(O)$_2$-NH-N=CH-(η^5-C_5H_4)]Fe(η^5-C_5H_5)}] (**4**) and the heterodimetallic compounds [Fe(η^5-C_5H_5){[(η^5-C_5H_4)-S(O)$_2$-NH-N=CH-(η^5-C_5H_4)]M(CO)$_3$}] with M = Re (**5a**) or Mn (**5b**). The X-ray crystal structures of compounds **3**, **5a** and **5b** are also reported. A comparative study of their electrochemical and spectroscopic properties is also described. Additional computational calculations based on DFT methodology have allowed us to elucidate the effect produced by the replacement of the terminal –NH_2 (in **2**) by the –N=CMe_2 (in **3**) and –N=CHR (in **4**, **5a** and **5b**)] moieties on the electronic distribution and to explain the differences detected in their electrochemical properties and absorption spectra. *In vitro* cytotoxic studies of compounds **2**, **4**, **5a** and **5b** on the HCT-116 (colon), MCF7 and MDA-MB231 (breast) cancer cell lines reveal that compound **2** had no significant activity (IC_{50} > 100 μM); while derivatives **4**, **5a** and **5b** resulted to be active in the three cancer cell lines selected in this study. The inhibitory growth potency of compounds **5a** and **5b** in the triple negative MDA-MB231 breast cancer cell line is similar (or slightly) greater than that of cisplatin. Moreover, Compounds **2**, **4**, **5a** and **5b** are less toxic than cisplatin in the normal and non-tumoural BJ fibrobasts and the heterodimetallic complexes **5a** and **5b** with selective index > 2.1 show an outstanding selective toxicity to the MDA-MB231 cancer cells.

Introduction

Cancer is the second leading cause of death in developed countries and its incidence rate is expected to raise.[1] The Global Cancer Observatory (GCO) estimates 29.5 million of new cancer cases in 2040 and more than 16 million deaths.[2] In addition to prevention, screening and new technological advances for its detection in earlier stages, more effective anticancer drugs and improved therapeutic protocols are needed to minimize the incidence rate and the morbidity.[3,4]

Molecular Hybridization Approach (MHA)[5-9] is a promising strategy to achieve new compounds with two (or more) subunits capable to block or inhibit the action of the key species (i.e. enzymes, proteins) involved and often overexpressed in the different stages of severe diseases[4-9]. The rational design of such compounds commonly known as "multi-targeted directed drugs"[6-8] is one of research areas with greatest future's expectations to get more effective chemotherapeutic agents.

It is well-known that: a) hypoxia modifies the microenvironment of solid tumours, affects the propagation of the initial tumour, the metastasis and, also induces chemo- and radio-resistance[3,9]; b) human carbonic anhydrase (hCA) isoform IX (hCA-IX) is overexpressed in hypoxic solid tumours with poor prognosis[3,9-11] and c) the inhibition of its catalytic activity delays the progression of the disease, and reduces the metastatic potential of several aggressive cancers[10,11]. Therefore, novel and potent hCA-IX inhibitors are gaining relevance in anticancer drugs (or prodrugs) design.[11] Sulfonamides and their derivatives are present in many commercial drugs and also in hCA inhibitors.[12,13] This is pushing the interest on new and small molecules with the "SO_2NH" unit as potential novel anticancer drugs.[14-16] Within the examples described so far, those shown in **Fig. 1** are especially relevant. The ureido-sulfonamide **A** (or "SLC-0111") is on clinical trials‡ and has synergic effect with

[a] *Laboratorio de Química Inorgánica y Organometálica, Departamento de Química Analítica e Inorgánica, Facultad de Ciencias Químicas, Universidad de Concepción, Edmundo Larenas 129, Casilla 160-c, Concepción, Chile. E-mail: rarancibia@udec.cl*
[b] *Université Lille Nord de France, Université Lille1, Unité de Catalyse et Chimie du Solide e UMR CNRS 8181, 59650 Villeneuve d'Ascq Cédex, France.*
[c] *Instituto de Química, Pontificia Universidad Católica de Valparaíso, Casilla 4059, Valparaíso, Chile.*
[d] *Departamento de Química de los Materiales, Facultad de Química y Biología, Universidad de Santiago de Chile, Casilla 40, Santiago, Chile.*
[e] *Biomed Division, LEITAT Technological Centre, Parc Científic de Barcelona, Edifici Hèlix, Baldiri i Reixach 13-21, 08028-Barcelona, Spain.*
[f] *Departament de Química Inorgànica i Orgànica, Secció de Química Inorgànica, Facultat de Química, Universitat de Barcelona, Martí i Franquès 1-11, E-08028 Barcelona, Spain. E-mail: conchi.lopez@qi.ub.es*

Electronic Supplementary Information (ESI) available: contains Supplementary Figures (**S1- 14**) and Tables (**S1-S7**). See DOI: 10.1039/x0xx00000x

View Article Online
DOI: 10.1039/D0DT01756F

conventional chemotherapeutic drugs.[15,16] Compound **B**, is a potent hCA-IX inhibitor, has a slightly greater antiproliferative effect on HeLa cells (IC_{50} = 25.2 μM) than cisplatin (IC_{50} = 28.9 μM) and induces apoptosis[17].

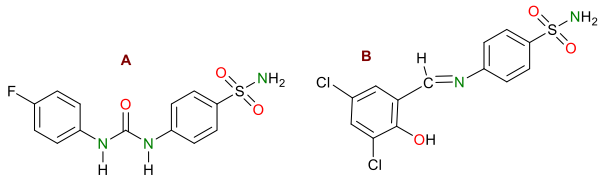

Figure 1. Two representative examples of potent CA-IX inhibitors with relevant anticancer activity.[15-17]

On the other hand, compounds with ferrocenyl units and/or [M{(η^5-C_5H_4R)}$(CO)_3$] (M = Re or Mn) arrays are attracting a great deal of interest due to their properties and applications.[18-22] Their lipophilicity, high stability, interesting electrochemical and photo-physical properties[19], low toxicity, together with their varied and outstanding biological activities (anticancer, antibacterial, antifungal, etc.), has increased their interest in *Medicinal Organometallic Chemistry* (MOC) as biosensors, bioprobes, for cellular imaging, etc,[18,23-25] and also as valuable cores in new drugs or prodrugs design.[23-25] During more than one decade we have focused our work in: a) ferrocene derivatives (i.e. imines, hydrazones), b) their use as metalloligands in front of transition metals [26-30] and, c) the study of their properties, applications and catalytic and biological activities.[26-34] So far, we have achieved compounds with low toxicity in normal and non-tumoural cells, potent inhibitory growth effect in several cancer cell lines and an example[31,32] that shows synergic effect with cisplatin and induces the nuclear translocation of FOXO 3a tumour supresor[32b].

More recently, we initiated a parallel study on cyrhetrene (M = Re) and cymantrene (M = Mn) derivatives as new anticancer or antiparasitic drug candidates.[27-30,33a,35] Compounds **C-F** in **Fig. 2**. are less toxic than cisplatin in normal and non-tumoural BJ cell lines. [35a] Aldimine **D**, showed an inhibitory growth potency higher than **C** and cisplatin in HCT116 and MBA-MD231 cell lines.[35a] Compound **E** was a more potent anticancer agent than **F** on MCF-7 cell lines, and showed no significant anti-*Trypanosoma cruzi* activity, while the Mn(I) derivative (**F**) resulted to be active. This suggested that the replacement of the Re(I) by Mn(I) produces significant changes in their anticancer or antichagasic activities and thus on their utility for the development of specific chemotherapeutic agents.[35b]

Despite of the increasing interest in: a) the use of the MHA to achieve new chemotherapeutic drugs[5-8], b) compounds with the "SO_2NHR" units and potent inhibitory effect on hCA-IX as promising candidates for new anticancer drugs[14-16] and, c) cyrhetrene, cymantrene and ferrocene derivatives in new drugs design[22-25], compounds containing "SO_2NHR" units and [M(η^5-C_5H_4R)$(CO)_3$] or ferrocenyl arrays are not common[36-40]. Compound **G** (**Fig. 3**) was described in 1958[36], but the remaining examples shown in **Fig. 3** (**H**-**M**) have been reported in the late five years[37-40]. Compounds **H** and **I** (**Fig. 3**), showed antitubercular activity on *M. tuberculosis mc²6230* strain, but the Re(I) complexes (**J**) were more active than their Fe(II) analogues (**I**)[38]. A few months ago, and in collaboration with Prof. C. T. Supuran's group some of us reported the set of compounds **L** and **K** (**Fig. 3**) with a potent inhibitory effect on several hCA isoforms[40].

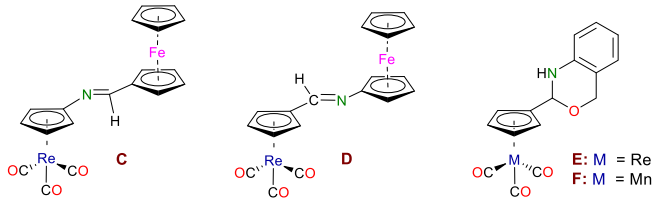

Figure 2. Hybrid cyrhetrenyl/ferrocenyl aldimines (**C** and **D**) and the 2,4-dihydro-1H-3,2-benzoxazines with a cyrhetrenyl (**E**) or cymantrenyl (**F**) group on position 2, with interesting biological activities.[35]

Due to the emerging interest on compounds with ferrocenyl or [M{(η^5-C_5H_4R)}$(CO)_3$] cores [M = Re(I) or Mn(I)] and the "SO_2NH" unit as hCA inhibitors and the lack of in vitro studies of their anticancer activity, in this paper we describe new types of small molecules in which the "SO_2NH" unit is attached to the ferrocenyl, cyrhetrenyl or cymantrenyl group (**2-5** in **Scheme 1**), together with comparative studies of their properties and cytotoxic activities in normal and non-tumoural cell lines and also in three cancer cell lines.

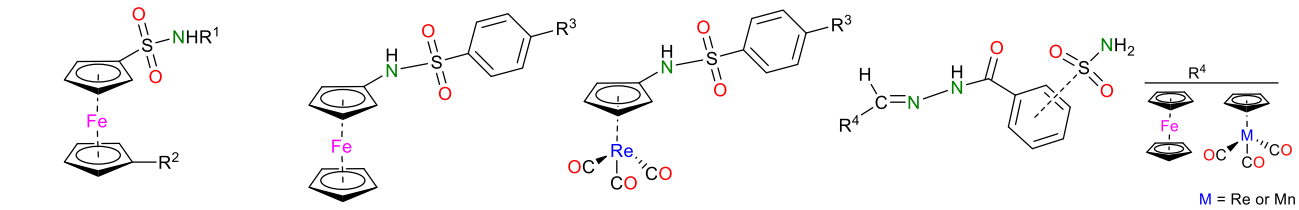

Figure 3. Representative examples of ferrocenyl, cyrhetrenyl or cymantrenyl compounds with one or two "SO_2NH" units.[36-40]

View Article Online
DOI: 10.1039/D0DT01756F

ARTICLE

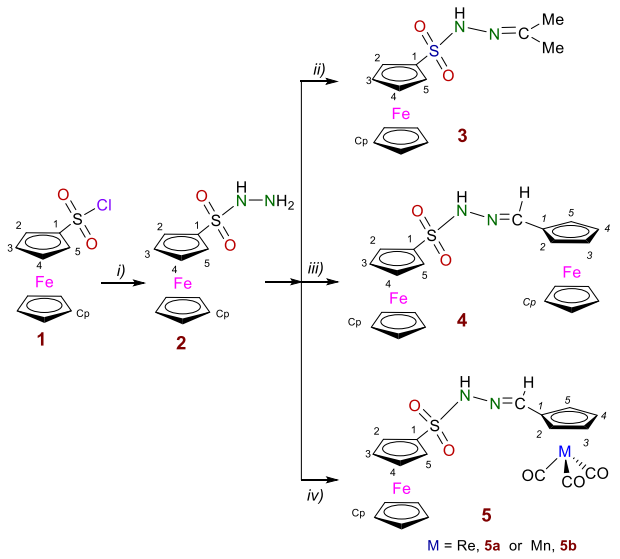

Scheme 1. Synthesis of the new compounds: *i)* hydrazine in THF, at room temperature; *ii)* in acetone at room temperature; *iii)* equimolar amount of ferrocenecarboxaldehyde in H_2O and in the presence of HCl at room temperature for 18h; *iv)* the same procedure as in *iii)*, but using the corresponding aldehyde $[M\{(\eta^5\text{-}C_5H_4)CHO\}(CO)_3]$, M = Re (for **5a**) or M= Mn (for **5b**).

Results and Discussion

Synthesis and characterization of compounds $[Fe(\eta^5\text{-}C_5H_5)\{(\eta^5\text{-}C_5H_4)S(O)_2NHNH_2\}]$ (2) and $[Fe(\eta^5\text{-}C_5H_5)\{(\eta^5\text{-}C_5H_4)\text{-}S(O)_2\text{-}NH\text{-}N{=}CMe_2\}]$ (3)

Treatment of ferrocenylsufonyl chloride (**1**)[41] with hydrazine in THF for 24 h gave, after concentration, a pale-yellow solid [**Scheme 1**, *i)*]. Its elemental analyses (see Experimental section) were consistent with those calculated for $[Fe(\eta^5\text{-}C_5H_5)\{(\eta^5\text{-}C_5H_4)\text{-}S(O)_2\text{-}NH\text{-}NH_2\}]$ (**2**) and its high resolution mass spectra (HRMS) and EI-mass agrees with the proposed structure. The IR spectrum of **2** showed the absorption bands due to the asymmetric and symmetric stretchings of the $-SO_2-$ array (at 1345 and 1148 cm^{-1}, respectively) and also, those due to the -NH- units (at 3361 and 3276 cm^{-1}). These two sets of bands are characteristic of sulfonylhydrazines[42].

Compound **2** is a stable solid at room temperature and exhibits high solubility in $CHCl_3$, CH_2Cl_2, DMSO and acetone. In view of this, and due to the scarcity of crystal structures of ferrocene derivatives with $-SO_2NHNH_2$ units, several experiments were carried out in order to achieve crystals suitable for X-ray analyses. Unfortunately, slow evaporation of $CHCl_3$ and CH_2Cl_2 solutions of compound **2** at different temperatures failed, but when these solvents were replaced by acetone, the formation of golden crystals was observed after evaporation of the solvent at 4 °C. However, the IR spectrum of these crystals was not coincident with that of **2** and showed a new intense and sharp band at 1637 cm^{-1}, typically assigned to the stretching of the >C=N- functional group. These findings suggested the formation of a new product (herein after referred to as **3**).

Characterization data of **3** and X-ray diffraction studies (see below) allowed us to identify it as $[Fe(\eta^5\text{-}C_5H_5)\{(\eta^5\text{-}C_5H_4)\text{-}S(O)_2\text{-}NH\text{-}N{=}CMe_2\}]$ that arises from the condensation reaction between the sulfonylhydrazine **2** and the acetone used as solvent.

Compound **3** could be isolated in fairly good yield by treatment of the starting material with a large excess of acetone (See *Experimental Section*) at room temperature [**Scheme 1**, step *ii)*]. These experimental conditions are similar to those required for the preparation of $R^5C_6H_4\text{-}S(O)_2\text{-}NH\text{-}N{=}CMe_2$ (with R^5 = 4-Me or 2-NO_2)[43], but milder (lower temperature and shorter reaction time) than those reported for $[Fe(\eta^5\text{-}C_5H_5)\{(\eta^6\text{-}C_6H_4R^6)\text{-}NH\text{-}N{=}CMe_2\}][PF_6]$ (R^6 = H or 4-Me)[44]. This result indicates that the $-NH_2$ group of **2** is more reactive than in $[Fe(\eta^5\text{-}C_5H_5)\{(\eta^6\text{-}C_6H_4R^6)\text{-}NH\text{-}NH_2\}]$.

The X-ray crystal structure of **3**‡ (**Table S1**) confirmed the presence of molecules of $[Fe(\eta^5\text{-}C_5H_5)\{(\eta^5\text{-}C_5H_4)\text{-}S(O)_2\text{-}NH\text{-}N{=}CMe_2\}]$ (**Fig. 4**).

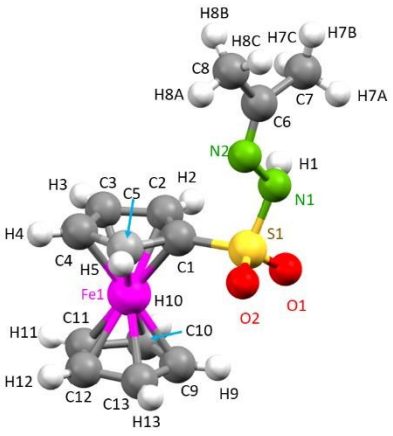

Figure 4. Molecular structure of $[Fe(\eta^5\text{-}C_5H_5)\{(\eta^5\text{-}C_5H_4)\text{-}SO_2\text{-}NH\text{-}N{=}CMe_2\}]$ (**3**). Selected bond lengths (in Å): S1-O1, 1.4327(18); S1-O2, 1.4220(19); S1-N1, 1.644(2); S1-C1, 1.739(2); N1-N2, 1.413(3); N2-C6, 1.270(3); C6-C7, 1.494(3); C6-C8, 1.492(3); Fe1-C_{ring} [average value (a.v.)]) 2.035(14), C-C (a.v. for the ferrocenyl unit), 1.405(34). Selected bond angles (in deg.): C1-S1-O1, 109.96(11); C1-S1-O2, 108.26(13); O1-S1-N1, 102.63(11); O2-S1-N1, 108.56(12); O2-S1-O1, 119.99(12); S1-N1-N2, 114.24(15); N1-N2-C6, 115.04(19); N2-C6-C7, 125.1(1) and N2-C6-C8, 117.4 (2). Selected torsion angles (in deg.): S1-N1-N2-C6, -170.32(16); S1-C1-C5-C4, 178.35(17); O1-S1-N1-N2, -179.65(16); O1-S1-C1-C2, -38.6(2); O1-S1-C1-C5, 144.5(2); O1-S1-N1-N2, -51.66(19); O2-S1-C1-C2, -171.45(19); O2-S1-C1-C5, 11.6(2); N1-N2-C6-C7, 2.1(3); N1-N2-C6-C8, -177.17(19) and C1-S1-N1-N2, 64.77(18).

View Article Online DOI: 10.1039/D0DT02765E

The N1-S1 bond length [1.644(2) Å] of **3** is very similar to those found in $R^5C_6H_4$-$S(O)_2$-NH-N=CMe_2 (with R^5 = 4-Me or 2-NO_2)[43], its C1-S1 bond is clearly shorter (1.739(2) Å than for its phenyl analogues (1.753 and 1.774 Å R^5 = 4-Me and NO_2 derivatives, respectively)[43,45]. This could be related to the different steric bulk of the C_5H_4 ring of **3** compared with the substituted phenyl ring in the $R^5C_6H_4$-$S(O)_2$-NH-N=CMe_2 derivatives[46].

As shown in **Fig. 4**, the O1 and O2 atoms are not coplanar with the C_5H_4 ring, they deviate from this plane by ca. 0.759 Å (for O1) and 0.181 Å (for O2) towards the Fe(II) ion. The plane defined by the set of atoms N1, N2 and C6, is nearly orthogonal to the substituted pentagonal ring (angle between their main planes = 89.9°). This arrangement is similar to that found for related compounds of general formulae R^1-SO_2-NH-NHR^2, with R^1 = substituted phenyl ring.[41,43]

In the crystals, two vicinal molecules assemble by dual cooperative N–H···O intermolecular interactions [**Fig. S1**, **A**)]. and the resulting units are connected by C-H ··· π short contacts [**Fig. S1**, **B**)].

Compounds **2** and **3** were also characterized in solution by NMR and UV-visible spectroscopies, but for comparison purposes, the results obtained from these studies will be presented and discussed later on.

In view of: a) the proclivity of **2** to react with acetone [**Scheme 1**, step *ii)*], b) the increasing interest on hydrazide derivatives and specially on sulfonylhydrazones in Medicinal Chemistry[46-49], c) the huge attraction of small molecules containing simultaneously biologically active groups as substituents (i.e. heterocycles) or linkers, and one or two ferrocenyl groups or additional cyrhetrenyl and cymantrenyl units[18-25,28-33,35-40] and d) the scarcity of compounds arising from the assembly of these organometallic units through a "–$S(O)_2$-NH-N=C<" connector, we also explored the reactivity of **2** in front of three organometallic aldehydes.

Homo- and Heterobimetallic compounds: synthesis and characterization

Treatment of **2** with equimolar amount of ferrocene carboxaldehyde [**Scheme 1**, step *iii)*] at room temperature for 18 h gave an orange microcrystalline solid whose characterization data (see *Experimental section*) agreed with those expected for homodimetallic sulfonylhydrazone [Fe(η^5-C_5H_5){[(η^5-C_5H_4)-$S(O)_2$-NH-N=CH-(η^5-C_5H_4)]Fe(η^5-C_5H_5)}] (**4**).

When ferrocenecarboxaldehyde was replaced by [M{(η^5-C_5H_4CHO)}$(CO)_3$] (M = Re or Mn) the corresponding heterodimetallic compounds [Fe(η^5-C_5H_5){[(η^5-C_5H_4)-$S(O)_2$-NH-N=CH-(η^5-C_5H_4)]M$(CO)_3$)}] {M = Re (**5a**) or Mn(**5b**) [**Scheme 1**, step *iv)*]}, were obtained in good yields (90 %) as whitish solids. Elemental analyses, HRMS and EI-mass spectra of **4**, **5a** and **5b** (see *Experimental section*) were consistent with their proposed formulae. Additional peaks arising from loss of the CO ligands attached to the M(I) atoms of **5a** and **5b** were also detected in their mass spectra.

The IR spectra of **4**, **5a** and **5b** exhibited the typical absorption bands due to the stretchings of the >C=N- (in the range 1585-1610 cm^{-1}) and >NH- units (at ca. 3146 cm^{-1}) of hydrazones with ferrocenyl, cyrhetrenyl or cymantrenyl units[21d-e,33b,34] as well as the those characteristic of the sulfonyl units (at around 1354 and 1194 cm^{-1}.[42] These findings confirmed the presence of the "-SO_2-NH-NH=CH-" bridge connecting the two organometallic fragments in **4**, **5a** and **5b**. As expected, the IR spectra of [Re(η^5-C_5H_4)$(CO)_3$] (**5a**) and its Mn (I) analogue (**5b**) also showed intense bands (in the range 2020-1930 cm^{-1}) due to the CO ligands.

Compounds **5a** and **5b** were also characterized by X-ray diffraction§ (**Table S1**) and their crystal structures confirmed the existence of [Fe(η^5-C_5H_5){[(η^5-C_5H_4)-$S(O)_2$-NH-N=CH-(η^5-C_5H_4)]M$(CO)_3$}] molecules with M = Re (in **5a**) or Mn (in **5b**). Despite these compounds differ exclusively in the nature of the metal ion (Re(I) in **5a** and Mn(I) in **5b**), their crystal structures show some interesting differences. First, crystals of **5a** contain only one type of molecules (**Fig. 5**), while those of **5b** have two (hereinafter referred to as **A** and **B**, **Fig. 6**). A selection of bond lengths and angles for **5a** and **5b** is included in the captions of **Figs. 5** and **6**, respectively.

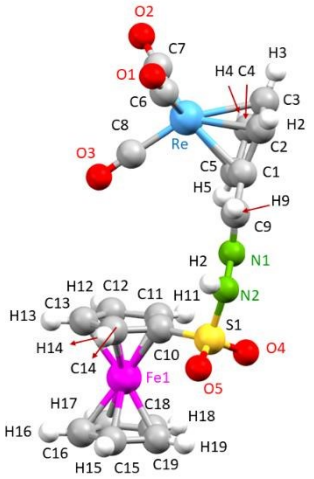

Figure 5. Molecular structure of **5a**. Selected bond lengths (in Å): S1-O4, 1.419(2); S1-O5, 1.436(2); S1-N2, 1.651(3); S1-C10, 1.724(3); N1-N2, 1.402(4); N2-C9, 1.257(4); Fe1-C_{ring} [average value, a.v.] 2.020(19); Re-C_{ring} (a.v.), 2.299(11); Re-C_{CO} (a.v.), 1.904(7); C-C_{ring} (a.v. for the cyrhetrenyl unit), 2.298(13); C-C_{ring}(a.v. for the ferrocenyl unit), 1.393(30). Selected bond angles (in deg.): C10-S1-O4, 109.39(11); C10-S1-O5, 109.10(15); O4-S1-N2, 107.37(15); O5-S1-N2, 103.17(14); O4-S1-O5, 119.60(15); N2-S1-C10, 107.44(15); S1-N2-N1, 113.1(2); N1-N2-C9, 115.3(3); N2-C6-C7, 119.6(15) and N2-C6-C8, 117.4 (2); N1-C9-C1, 119.2(3); Selected torsion angles (in deg.): N2-N1-C9-C1, 179.4(4); S1-N2-N1-C9, 167.7(4); C10-S1-N2-N1, -56.6(4); O4-S1-N2-N1, 61.02; O5-S1-N2-N1, 171.7(4); C11-C10-S1-N2, 93.4(4) and C14-C10-S1-N2, -87.2(5)

As shown in **Figs. 5** and **6** the "M$(CO)_3$" units are located on the same side as the "Fe(η^5-C_5H_5)" array and opposite to the oxygen atoms of the SO_2 unit. In both cases, the pentagonal rings of the cyrhetrenyl or cymantrenyl units are planar and twisted in relation to the substituted ring of the ferrocenyl unit (angles between their main planes being 70.8° (in **5a**) and 60.1° and 63.3° (in molecules **A** and **B**, respectively of **5b**). The relative orientation of these two rings is similar to those found in the sulfonylhydrazones of general formulae: $R^1C_6H_4$-SO_2-NH-N=CH-($C_6H_4R^2$) with R^1 = H, NO_2, Cl and R^2 = H or Me.[43,49]

View Article Online
DOI: 10.1039/D0DT01756E

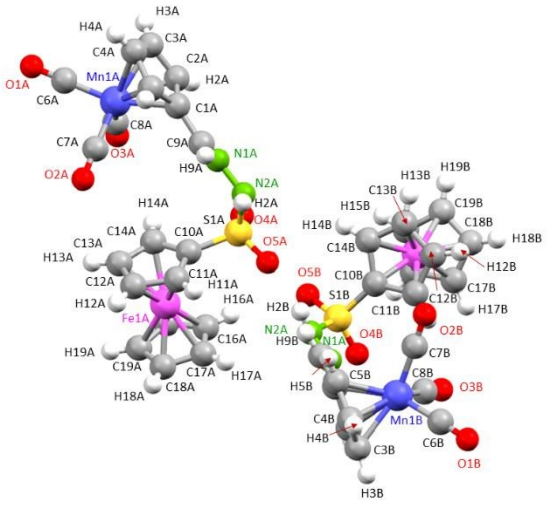

Figure 6. Molecular structure of **5b**. Selected bond lengths (in Å) in molecule **A**: S1A-O4A, 1.4222(14); S1A-O5A, 1.4326(14); S1A-N2A, 1.6527(15); S1A-C10A, 1.7301(19); N1A-N2A, 1.402(4); N1A-C9A, 1.268(2); C9A-C1A, 1.460(2); Mn1A-C_{ring}[average value (a.v.)], 2.137 (7); Mn1A-C_{CO}(a.v.), 1.787(9); Fe1A-C_{ring} (a.v.), 2.034(17); and C-C_{ring} (a.v. for the ferrocenyl unit), 1.406(18); in molecule **B**: S1B-O4B, 1.4219(14); S1B-O5B, 1.4350(13); S1B-N2B, 1.6507(14); S1B-C10B, 1.7274(17); N1B-N2B, 1.3981(19);N1B-C9B, 1.271(2); C9B-C1B, 1.463(2); Mn1B-C (a.v.), 1.792(3); Fe1B-C_{ring} (a.v.), 2.039(14); and C-C_{ring} (a.v. for the ferrocenyl unit), 1.411(14). Selected bond angles (in deg.): in molecule **A**: C10A-S1A-O4A, 109.51(9); C10A-S1A-O5A, 108.82(10); O4A-S1A-N2A, 108.45(9); O5A-S1A-N2A, 102.59(8); O4A-S1A-O5A, 120.20(10); N2A-S1A-C10A, 106.28(8); N2B-S1B-C10B, 106.53(8); S1A-N2A-N1A, 114.41(11); N1A-N2A-C9A, 115.93(15); In **B**: C10B-S1B-O4B, 110.28(9); C10B-S1B-O5B, 108.00(9); O4B-S1B-N2B, 108.15(8); O5B-S1B-N2B, 102.60(8); O4B-S1B-O5B, 120.28(9); S1B-N2B-N1B, 116.35(11); and N1B-N2B-C9B, 115.44(14). Selected torsion angles (in deg.): molecule **A**: N2A-N1A-C9A-C1A, 124.29(11); S1A-N2A-N1A-C9A, 140.21(10); C10A-S1A-N2A-N1A, -65.65(11); O4A-S1A-N2A-N1A, 52.05(11); O5A-S1A-N2A-N1A, 179.78(10); C11A-C10A-S1A-N2A, 79.20(11) and C14A-C10A-S1A-N2A97.47(11) and in molecule **B**: N2B-N1B-C9B-C1B, 179.88(11); S1B-N2B-N1B-C9B, 145.68(10); C10B-S1B-N2B-N1B, 74.84(11); O4B-S1B-N2B-N1B, 43.68(11); O5B-S1B-N2B-N1B, 171.77(11); C11B-C10B-S1B-N2B, 88.37(11) and C14B-C10B-S1B-N2B, 179.88(11).

In **5a** and **5b** (**Figs. 5** and **6**) the amine nitrogen and the "[M{(η^5-C_5H_4)}$(CO)_3$] unit are in a trans- arrangement [torsion angle N2-N1-C9-C1 in **5a** = 179.7°) and its analogues in molecules **A** and **B** of **5b** are 174.3° and 171.8°, respectively), thus confirming that in both compounds the hydrazone adopts the *E*- form in the solid state.

The presence of only one type of molecules of **5a** and two (**A** and **B**) of **5b** in the crystals produces significant variations in the assembly of the structural units. (**Fig. S2** and **S3**).

It should be noted that no significant variation in either the physical appearance or the IR spectra of freshly prepared solid samples of compounds **2-5** and after several weeks of storage at room temperature. Thus, suggesting that these new products exhibit high stability in the solid state.

NMR studies.

The new compounds presented in this work were also characterized in solution by ^{1}H and ^{13}C{^{1}H}-NMR. For compounds **4**, **5a** and **5b** the spectra were registered in acetone-d_6 at 298 K, but for **2**, that reacts with acetone even at room temperature, the solvent used was $CDCl_3$ (NMR data is presented in the *Experimental section*).

The ^{1}H -NMR spectrum of compound **2** exhibits two singlets at δ = 3.62 and 5.40 ppm, due to the protons of the –NH-NH_2 unit and the typical pattern of monosubstituted ferrocene derivatives, that consists of three signals of relative intensities 5:2:2 in the range 4.40-4.80 ppm, assigned to the protons of the C_5H_5 ring and to the two pairs of non-equivalent protons [(H^2, H^5) and (H^3, H^4)] of the substituted ring. For compound **4**, an additional set of signals with identical pattern appeared also in the same region, but slightly shifted to higher fields.

The ^{1}H-NMR spectra of the bimetallic compounds **4**, **5a** and **5b**, showed two singlets (one at $\delta \approx$ 9.8 ppm and the other in the range 7.5-7.9 ppm) due to the protons of the –NH-N=CH- functional group. For compounds **5a** and **5b**, the signals due to the pairs of protons (H^2, H^5) and (H^3, H^4) of the cyrhetrenyl and cymantrenyl arrays appeared at intermediate fields [$5.0 \leq \delta \leq$ 6.5 ppm in the ^{1}H-NMR spectra.

^{13}C{^{1}H}-NMR spectra of the new compounds showed some common features due to the presence of the "[Fe(η^5-C_5H_5){(η^5-C_5H_4)-SO_2NH-"}] unit. In all cases, four signals were detected in the range 68-90 ppm, of which the most intense is due to the carbon nuclei of the (C_5H_5) ring; the less intense one is assigned to the *ipso* carbon atom of the other ring (C^1); while the remaining two correspond to the two pairs of non-equivalent atoms of this ring [(C^2 and C^5) and (C^3 and C^4)].

For compounds **4**, **5a** and **5b** the remaining resonances detected in the range 65.0-100.0 ppm were assigned to the ^{13}C nuclei of the other ferrocenyl unit of **4** or the [M(η^5-C_5H_4)] arrays of **5a** and **5b**. It should be noted that the position of the signal due to the imine carbon of **4-5** and those of the CO ligands of compound **5a**, agreed with those reported previously for closely related ferrocenyl, cyrhetrenyl and cymantrenyl derivatives [26a,26g,27,31c,32a,33].

These NMR studies provided conclusive evidences of the presence of only one isomer of compounds **4**, **5a** and **5b** in acetone-d_6 at room temperature. The position of the signals due to the imine proton and carbon nuclei agree with other hydrazones with the *E*- form[33b]. The use of molecular models revealed that a *cis*- arrangement of the substituents (*Z*- form), would induce strong steric hindrance between the organometallic group and the NH unit. On this regard, we assume that these compounds adopt the *E*- form in acetone-d_6. Moreover, comparison of data (see *Experimental section*) allowed us to deduce the effect produced by the organometallic substituents bound to the imine carbon on the -SO_2-NH-N=CH- moiety. The replacement of the [M{(η^5-C_5H_4)}$(CO)_3$] arrays of **5a** and **5b** by the ferrocenyl unit to give **4**, produces a highfield shift ($\approx$ 0.55 ppm) of the resonance of the NH proton and the opposite trend is found for the chemical shift of the imine carbon. These trends, that agree with those observed for ferrocenyl and cyrhetrenyl hydrazones, as well as 1,3,4-thiadiazole derivatives[30a] and related Schiff base derivatives, have been attributed to the different electron-donor abilities of the ferrocenyl and electron-acceptor of the [M(η^5-C_5H_4)CO_3] (M

= Re or Mn) units[33b,35]. Computational studies described below confirm this hypothesis.

NMR has also been a powerful tool to test the stability of the new compounds **4-5** in other solvents (i.e. acetonitrile, DMSO and mixtures DMSO:D_2O) used for additional studies described in the following sections.

Since the electrochemical studies were carried out in acetonitrile, we registered the ^{1}H-NMR spectra of compounds **2**, **3**, **4**, **5a** and **5b** in CD_3CN (**Figs. S4-S7**) at room temperature. In all cases the spectra showed only one set of resonances, the number of signals observed in the spectra and their multiplicities were consistent with those expected, and no evidences of the presence of any other species in solution were detected. Besides these, ^{1}H-NMR spectra obtained after several hours of storage at room temperature was coincident with that obtained for the freshly prepared samples. This finding suggests that compounds **2**, **3**, **4**, **5a** and **5b** were also stable at room temperature in CD_3CN solutions.

As mentioned above sulfonyl-hydrazone derivatives are especially attractive for new drugs development. However, in this context, in addition to their potential biological activities other properties should be considered and specially their stability in the solid state and also in solution. Compounds **2-5** exhibited high stability in the solid state. In view of this, and since for the biological studies described below, the first step consisted in the dissolution of the compound in DMSO, followed by subsequent dilutions with water, additional NMR studies were carried out in order to evaluate the stability of the new products in DMSO-d_6.

The ^{1}H-NMR spectra of freshly prepared solutions of compounds **4**, **5a** and **5b** in DMSO-d_6 showed one set of resonances. (**Figs. S8-S10**) indicating the presence of only one specie in solution. Moreover, the comparison of these spectra with those obtained after several periods of storage (*t*) at 298 K, reveal that compound **4** is highly stable under these conditions since no significant change was observed in the spectra registered at *t* = 0 and after 72 h. The behaviour of compounds **5a** and **5b** is a bit different. As shown in **Figs. S9** and **S10**, a broadening of the signal due to the amine proton was observed even after 24 h of storage. This could be attributed to an exchange process, commonly observed for hydrazone derivatives[51] and the comparison of results suggests that the N-H bond of **5a** and **5b** is more prone to exchange than in the bis(ferrocenyl) derivative **4**. For *t* = 72 h the main set of resonances observed in the spectra agreed with those of compounds **5a** and **5b**, but additional signals with extremely low intensity were also detected in the spectra, thus indicating the presence of minor species in solution.

In order to evaluate the effect of water, ^{1}H-NMR spectra of freshly prepared solutions of **4**, **5a** and **5b** in a DMSO-d_6:D_2O (1:1) mixture were registered. Comparison of these spectra (**Figs. S11-S13**) with those in DMSO-d_6 (**Figs. S8-S10**) revealed that: a) for compound **4**, the signals became broader than in DMSO-d_6 and some of the resonances overlapped, and b) in the ^{1}H-NMR spectra of **4** and **5b**, the resonance of the -NH proton was not detected, while for **5a**, it was still observed but with extremely low intensity. Besides these, additional signals with low intensity also suggested the coexistence of minor species in solution. Finally, the spectra shown in **Fig. S12**, also suggest that the relative abundance of the minor component does not vary significantly after 72 h of storage at 298 K. [#]All these studies indicate that compounds **4**, **5a** and **5b** are fairly stable in DMSO-d_6:D_2O (1:1) mixtures.

Study of the effect of the substituents on the properties of the new compounds

Electrochemical studies. In a first attempt to elucidate the effects produced by the organometallic substituents (R = ferrocenyl, cyrhetrenyl, cymantrenyl) in the electronic environment of the Fe(II) centre of the novel ferrocenylhydrazones: [Fe(η^5-C_5H_5){(η^5-C_5H_4)-S(O)$_2$-NH-N=CHR}] we decided to explore their electrochemical properties. For comparison purposes compounds **2** and **3** were also included in this study.

The electrochemical studies were carried out by cyclic voltammetry of freshly prepared solutions (10^{-3} M) in acetonitrile with (Bu_4N)[PF_6] as the supporting electrolyte. All these experiments were carried out at a scan rate ν = 100 mV × s^{-1}. The cyclic voltammograms (hereinafter referred to as CVs) obtained at 298 K are depicted in **Fig. 7** together with the labels used to identify the peaks. A summary of the most relevant electrochemical data is presented in **Table 1**.

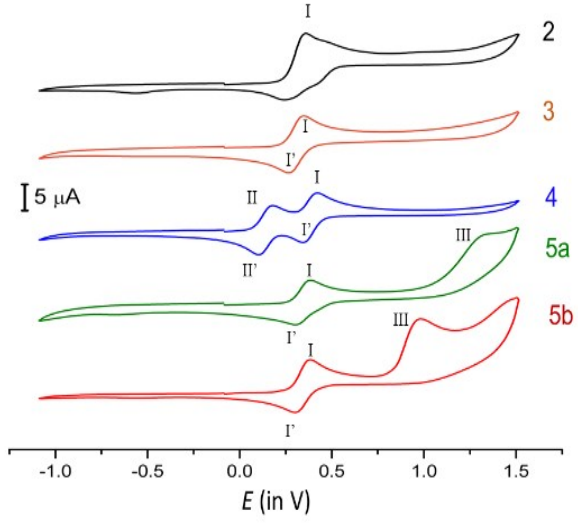

Figure 7. Cyclic voltammograms of compound: [Fe(η^5-C_5H_5){(η^5-C_5H_4)-S(O)$_2$-NH-NH_2}] (**2**) and the new sulfonyl hydrazones of general formulae: [Fe(η^5-C_5H_5){(η^5-C_5H_4)-S(O)$_2$-NH-N=CMe_2}] (**3**) and [Fe(η^5-C_5H_5){(η^5-C_5H_4)-S(O)$_2$-NH-N=CHR}] with R = ferrocenyl (**4**), cyrhetrenyl (**5a**) or cymantrenyl (**5b**) in the range of potentials: -1.20 ≤ *E* ≤ 1.5 V, at a scan rate = 100 mV/ s, together with the labelling system used for the observed peaks.

As shown in **Fig. 7**, the CVs of the monoferrocenyl derivatives **2**, **3**, **5a** and **5b** showed one anodic peak (I) in the range 0.30 - 0.50 V. A directly associated and well-defined reduction (I') peak in the reverse scan was also observed for [Fe(η^5-C_5H_5){(η^5-C_5H_4)-S(O)$_2$-NH-N=CMe_2}] (**3**) and the dimetallic derivatives **5a** and **5b**.

View Article Online
DOI: 10.1039/D0DT01756F

Therefore, the oxidation peak I can be assigned to the oxidation of the ferrocenyl group attached to the -S(O)$_2$- unit. Molecular orbital (MO) calculations (see below) confirm this hypothesis.
The sulfonyl hydrazones **3**, **5a** and **5b**, differ exclusively in the nature of the substituent attached to the imine carbon, which is rather far (at a five bond lengths distance) from the Fe(II) centre. This could explain why for the cyrhetrenyl (**5a**) and cymantrenyl (**5b**) derivatives the position their anodic and cathodic peaks (**I** and **I'**, respectively) are very similar (**Table 1**). For compounds **2** and **3**, the anodic peak is slightly shifted (≈ 23 mV) in relation to those of compounds **5a** and **5b**.

Table 1. Summary of electrochemical data [anodic (E_{pa})^i, cathodic (E_{pc})^i potentials and the separation between peaks $[\Delta E = (E_{pa})_I - (E_{pc})_{I'}]$ for the new compounds in V. Data were obtained at a scan rate υ = 100 mV s^{-1} and referenced to the ferrocene/ferricinium couple (Fc/Fc^+) (for the identification of peaks see **Fig.7**)

	Oxidation scan			Reverse Scan			
	I	**II**	**III**	**I´**	**II´**	ΔE^a	$E_{1/2}$
2	0.357	———	———	0.266	———	0.091	0.312
3	0.348	———	———	0.267	———	0.081	0.301
4	0.423	0.181	———	0.342	0.105	0.081 0.076^b	0.383 0.143^b
5a	0.380	———	1.307	0.305	———	0.075	0.343
5b	0.382	———	0.982	0.302	———	0.080	0.342

^{a} Except where quoted these values refer to the peaks **I** and **I'**. ^{b} For peaks **II** and **II'**.

The cyclic voltammograms of compound **4**, with two ferrocenyl units, is more complex than those of **2**, **3**, **5a** and **5b**. Two clear and well-defined waves were observed (**Fig. 7**). One of them in the same region as for compounds **2**, **3**, **5a** and **5b**, but slightly shifted (≈ 40 mV) to higher potentials, while the other one appeared in the range of potentials 0.10 V ≤ E ≤ 0.25 V.
The separation the anodic and cathodic potentials of the two waves (**Table 1**) depart from the constant value of 59 mV (theoretically expected for an electrochemically reversible one-electron step oxidation-reduction process)[52], suggesting that: a) the electron transfer at the electrode surface is slow compared to mass transport and / or b) there is a structural reorganization after the oxidation[26,31].
Compounds **4**, **5a** and **5b**, belong to the series [Fe(η^5-C_5H_5){(η^5-C_5H_4)-S(O)$_2$-NH-N=CHR}] and differ exclusively in the R group which is quite far away from the Fe(II) centre. On this basis, the replacement of the cyrhetrenyl (in **5a**) or cymantrenyl (in **5b**) units by the ferrocenyl moiety to give **4**, is not expected to produce big changes on the position of the wave involving the Fe(II) centre of the [Fe(η^5-C_5H_5){(η^5-C_5H_4)-S(O)$_2$- and its anodic potential. In view of these, we assumed that for complex **4**, the wave observed at lower potentials should be attributed to the oxidation-reduction process involving the ferrocenyl unit attached to the imine carbon. Computational studies described below confirmed this hypothesis. It should be noted that once this unit has oxidized, the subsequent removal of an additional electron requires higher potential than the oxidation of the ferrocenyl unit of compounds **3**, **5a** and **5b**.
Finally, it should be noted that the cyclic voltammograms of compounds **5a** and **5b**, exhibit an additional and poorly resolved oxidation peak (**III**). For **5a**, this peak appears in the range reported for other cyrhetrene derivatives and its potential (E_{pa}^{III} = 1.307 V) is similar to that reported for [Fe(η^5-C_5H_5)(η^5-C_5H_4)-CH=N-R] with R = [Re(η^5-C_5H_4)(CO)$_3$] (E_{pa} = 1.297 V)[35a] and assigned to the oxidation of the Re(I) metal ion.
For the Mn(I) analogue **5b**, the potential of peak **III** (E_{pa}^{III} = 0.982 V) is greater than those of the aldehyde [Mn{(η^5-C_5H_4)-CHO}(CO)$_3$] (E = 0.92 V)[53] and the 2-cymantrenyl-2,4-dihydro-1H-3,1-benzoxazine (E = 0.942 V) recently reported[35b], and proximal to the lowest values of triazoles with pendant cymantrenyl units (1.00 V ≤ E ≤ 1.37 V)[30a].
When the CV's were registered at different scan rates (ν = 50, 100 and 250 mV/s, **Fig. S14-S16** no significant variation was observed in the position of the peaks. This is consistent with chemical and electrochemical reversibility and also suggests a two sequential electron transfer reversible process (EE) for compound **4**. For **5a** and **5b**, where dimerization is important, the electrochemical studies suggest an EEC type process. The cyclic voltammogram of compound **5a** at ν = 250 mV / s (**Fig. S15**) shows a peak at ca. -0.6 V due to the reduction of the Re-dimer that supports the hypothesis.

Ultraviolet-visible studies. Absorption spectra of CH_2Cl_2 solutions of the new sulfonyl derivatives **2-4**, **5a** and **5b** were registered at 298 K. The UV-vis. spectra are shown in **Figure 8** and a summary of spectroscopic data is presented in **Table 2**.
In all cases the spectra (**Figure 8**) showed intense absorption bands (3.0 < log ε < 4.3) in the range 220 – 320 nm. One of them at λ_1 = 228 nm and in most of the cases presence of a shoulder at around 261 nm was also observed, except for complex **5a**, for which the position of a maximum or even the detection of a shoulder was not clear in the spectrum (**Fig. 8**).

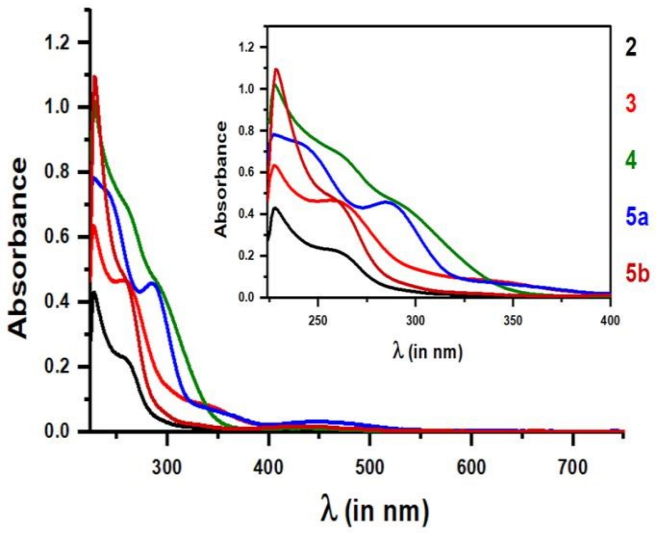

Figure 8. Ultraviolet-visible spectra of compounds **2-4**, **5a** and **5b** in CH_2Cl_2 at room temperature.

View Article Online
DOI: 10.1039/D0DT01765E

The UV-vis. spectra of compounds under study are more complex than those of ferrocenyl, cyrhetrenyl or cymantrenyl hydrazones of general formulae: R^7-CH=N-NH (4-NO_2-C_6H_4) that showed an intense band ($4.1 < \log \varepsilon < 4.5$) in the range 380-415 nm[33b]. Finally, it should be noted that for compounds **3**, **5a** and **5b** additional and weaker bands (with $\log \varepsilon$ in the range 2.5 - 3.2) were also observed at higher wavelengths ($320 < \lambda < 450$ nm) (**Table 2**).

Computational studies described in the following section have allowed us to assign the bands observed and to explain the complexity of UV-vis. spectra.

Table 2. Summary of experimental ultraviolet-visible spectroscopic data: position of the bands detected [wavelengths λ_i (in nm)] and logarithms of their molar extinction coefficients $\log \varepsilon_i$ in parenthesis for compounds **2-4**, **5a** and **5b** (see also **Fig.7**).

Compounds	λ_1 ($\log \varepsilon_1$)	λ_2 ($\log \varepsilon_2$)	λ_3 ($\log \varepsilon_3$)	λ_4 ($\log \varepsilon_4$)
2	228 (3.9)	262(3.6)	————	————
3	228 (4.1)	262(4.0)	345(3.2)	————
4	228(4.3)	261 [a]	294 (3.9)	————
5a [b]	228 (4.2)	244(4.2)	286 (4.0)	347(3.2)
5b	228 (4.3)	260 (4.2)	327(2.7)	451 (2.5)

[a] In this case the position of the maximum cannot be clearly identified (see **Fig. 8**).[b] Additional band at 448 nm ($\log \varepsilon_i = 2.8$).

Computational studies.

Sulfonamides and sulfonyl hydrazides and hydrazones are one of the most important types of organic compounds due to their outstanding properties, their rich reactivity, their utility as ligands in Coordination and Organometallic Chemistry and their multiple applications in a variety of fields, including medicinal chemistry.[14,15,40a,42,43,47-54] It is well-known that their properties and chemical reactivity (i.e. their capability to act a ligands in front of transition metal ions) are strongly dependent on the electronic distribution, the neat charges on the atoms involved in their functional groups, the topologies of the frontier orbitals and also their energies. In view of these and in order to elucidate the effect of the substituents on the imine carbon atom {(two Me in **3**), a ferrocenyl (in **4**), a cyrhetrenyl (in **5a**) or a cymantrenyl (in **5b**) unit} on the electronic distribution, theoretical studies based on Density Functional Theory (DFT) on compounds **3**-**5** were carried out and for comparison purposes the sulfonylhydrazine **2** was also included.

These calculations were carried using Q-Chem 5.1[55] included in the *Spartan 18* computer program[56] and the B3LYP hybrid functional[57]. Further details on the basis set used for all atoms are given in the experimental section.

In a first stage, geometries of compounds **2**-**4**, **5a** and **5b**, were optimized without imposing any restriction. Final atomic coordinates for the optimized geometries are included as supplementary information, (**Tables S2-S6**).

Bond lengths and angles of the optimized geometries of **3**, **5a** and **5b** were consistent with those obtained from the X-ray studies (the differences did not clearly exceed 3σ) and those of **2** and **4** are in the range reported for ferrocenyl Schiff bases[45].

Frontier orbitals [HOMO-1, HOMO, LUMO and LUMO+1] for compounds **2** and **3** are shown in **Figure 9** and those of the dimetallic derivatives (**4**, **5a** and **5b**) are presented in **Figure 10**. For compounds **2**, **3**, **5a** and **5b**, the HOMO-1 and HOMO are mainly centred on the (η^5-C_5H_5)Fe(η^5-C_5H_4) moiety; while for the bis(ferrocenyl) derivative **4**, these two molecular orbitals are mainly located on the other ferrocenyl unit which is attached to the imine carbon. In the HOMO orbital of **4**, there is also a tiny contribution of the imine unit.

Since it is widely accepted that the oxidation of a compound requires the removal of the electron from its HOMO orbital, the results obtained from the MO calculations, suggest that for compounds **2**, **3**, **5a** and **5b**, the first oxidation occurs on the ferrocenyl group bound to the sulfur; while for compound **4**, takes place on the other one. This explains the differences detected in cyclic voltammograms of compounds **2**, **3**, **5a** and **5b**, when compared with that of **4**. For the bis(Ferrocenyl) derivative **4** the first oxidation occurs at lower potentials than for **2**, **3**, **5a** and **5b** which are more resistant to oxidation than **4**. It is well-known that the proclivity of ferrocene derivatives to oxidize is strongly dependent on the electron donor/ withdrawing nature of the substituents. In general, those with electron donor groups are less resistant to oxidize than their analogues with electron pulling substituents[18a-b,26b-e,35a-b]. Therefore, the results obtained from the electrochemical studies and the MO calculations allow us to conclude that the -SO_2-NH-N=CHR group has a stronger electron-withdrawing ability than the -CH=N-NH-SO_2R one.

As shown in **Fig.9** the LUMO of compounds **2** and **3** is mainly centred on the ferrocenyl unit and the -SO_2- unit with a tiny contribution of the nitrogen; while for the dimetallic derivatives **4-5** (**Fig.10**) the main contribution arises from the hydrazone functional group and the ferrocenyl (in **4**) or [M{(η^5-C_5H_4)}$(CO)_3$] [M = Re (**5a**) or Mn(**5b**)] arrays attached to the imine carbon.

The calculated energies of the frontier orbitals [HOMO-1, HOMO, LUMO and LUMO+1] together with the energy gaps [E_{gap} = *E*(LUMO) - *E*(HOMO)] are presented in **Table 3** Comparison of data reveals that the values of E_{gap} increase according to the sequence **5a** < **5b** < **4** << **3** < **2**.

Table 3. Calculated energies (in eV) for the frontier orbitals [HOMO-1, HOMO, LUMO and LUMO+1) for compounds **2**-**4**, **5a** and **5b,** together with the energy gap [E_{gap} = *E*(LUMO) – E(HOMO)].

MO	**2**	**3**	**4**	**5a**	**5b**
LUMO+1	-0.40683	-0.15201	-0.33446	-1.00954	-0.84928
LUMO	-0.54036	-0.29670	-0.92443	-1.54955	-1.50860
HOMO	-5.74406	-5.52223	-5.35119	-5.67207	-5.66131
HOMO-1	-5.77414	-5.54001	-5.41609	-5.68921	-5.67370
E_{gap}	5.2037	5.2255	4.42670	4.12125	4.1527

View Article Online
DOI: 10.1039/D0DT01756F

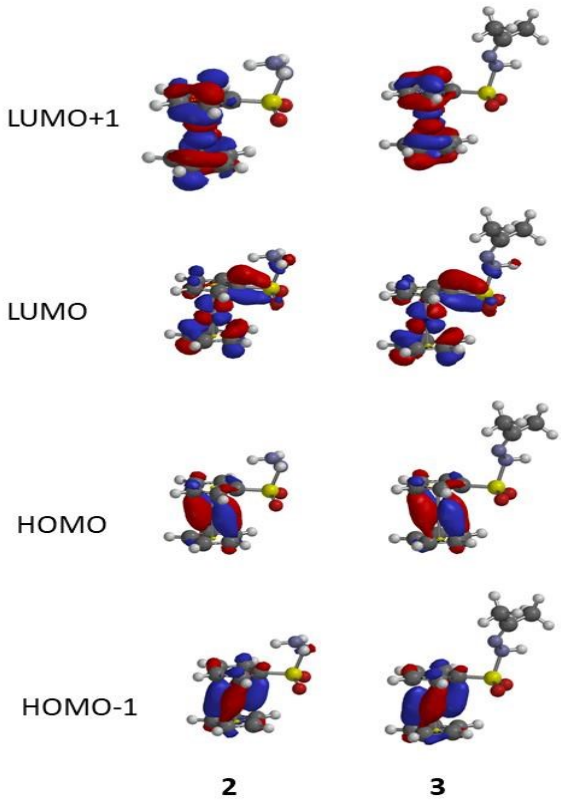

Figure 9. Frontier orbitals [HOMO-1, HOMO, LUMO and LUMO+1] of the ferrocenylsulfonyl hydrazine [Fe(η^5-C_5H_5){(η^5-C_5H_4)-S(O)$_2$-NH-NH$_2$}] (**2**) and [Fe(η^5-C_5H_5){(η^5-C_5H_4)-S(O)$_2$-NH-N=CMe$_2$}] (**3**).

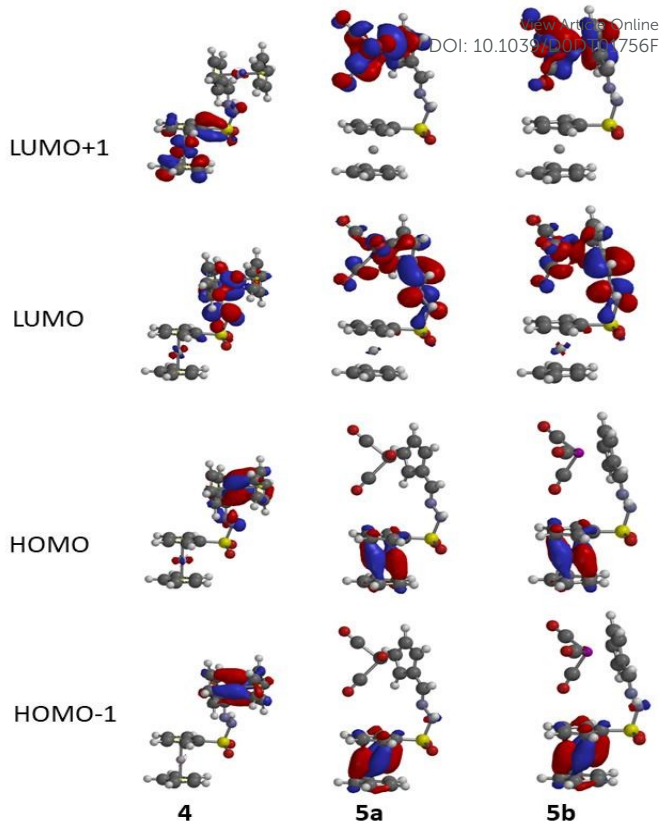

Figure 10. Frontier orbitals [HOMO-1, HOMO, LUMO and LUMO+1] for the dimetallic compounds [Fe(η^5-C_5H_5){(η^5-C_5H_4)-S(O)$_2$-NH-N=CHR] and R = {Fe(η^5-C_5H_5)(η^5-C_5H_4)} (**4**), [Re(η^5-C_5H_4)(CO)$_3$] (**5a**) or [Mn(η^5-C_5H_4)(CO)$_3$] (**5b**).

In compounds **2** and **3** the LUMO+1 is a π^* orbital of the ferrocenyl unit; while in **5a** and **5b** the major contributions of this orbital arise from the [M{(η^5-C_5H_4)}(CO)$_3$] moieties. The LUMO+1 orbital of **4** is markedly different from those of **5a** and **5b** and quite similar to the LUMO of **2** and **3**. It is noteworthy to mention that the energetic level of the LUMO+1 of compounds **2** and **3** is quite close to that of their LUMO orbitals [*E*(LUMO+1)- *E*(LUMO) < 0.16 eV), but for the bimetallic compounds the differences between the LUMO and LUMO+1 energetic levels increase to ca. 0.54 eV (for **5a**), 0.59 eV (for **4**) and 0.66 eV (for **5b**). The differences detected in the frontier orbitals of compounds **2-5** and in their energetic levels may affect the number of electronic transitions and their energies, and consequently their absorption spectra. In order to clarify this point and to explain the origin of the broad and intense bands detected in the UV-vis. spectra, the excitation energies and the oscillator strengths were calculated in CH_2Cl_2 (**Table S7**).

The results obtained revealed that the main absorption bands in the range 220 – 320 nm result from a large number of monoelectronic transitions that take place in a narrow range of energies. This could explain the broadening of the bands and the poor resolution of the spectra in this region.[Υ] The computational studies also reveal that absorption bands observed in the UV-vis. spectra of compounds **5a** and **5b** at 347 and 327 nm, respectively arise mainly from the HOMO → LUMO transition in both cases, but for **5b** energy of this transition is rather close to the HOMO-1 → LUMO.

Biological studies.

As mentioned above organometallic compounds with pendant ferrocenyl or [M{(η^5-C_5H_4R)}(CO)$_3$] groups and a biologically active units are attracting more and more interest in Medicinal Chemistry and specially in new drugs (or prodrugs) design and development.[21-25,27,29-32,33a,35,39] Except for compound **2**, the remaining products presented in this work (**3**, **4**, and **5a** and **5b**), belong to the family of products $R^1S(O)_2$-NH-N=CHR^2. Compounds of this kind with potent anticancer, antiparasitic, activities among others biological activities have been described.[40,42,47-49]

In view of these findings, and the ongoing interest on sulfonylamine derivatives as hCA inhibitors and their potential

as anticancer new drugs, we decided to check the potential biological activity of four of the new products (**2**, **4**, **5a** and **5b**). Compound **3** was not included in this study due to its low stability in DMSO-solutions, that reduces significatively its potential use in drugs design.

In a first stage, we evaluated the cytotoxic activities compounds (**2**, **4**, **5a** and **5b**) on the HCT-116 cancer cell line and compared them with that of cisplatin under identical experimental conditions. A summary of the results obtained for these studies is presented in **Table 4** and **Figure 11**.

Table 4. Cytotoxic activities of the new compounds **2**, **4**, **5a** and **5b** and cisplatin (IC_{50} values in μM) against the HCT-116 (colon), the MCF7 (breast) and the triple negative MDA-MB231 (breast) cancer cell lines together with the values obtained in the normal and non-tumoural human skin fibroblast BJ cell line. For comparison purposes, values obtained for cisplatin under identical experimental conditions are also given.

	Cytotoxic activities IC_{50} values in			
	Cancer cell lines			Normal and non-tumoural
	HCT116	MCF7	MDA-MB231	BJ
2	> 100	> 100	> 100	>100
4	55 ± 9	42 ± 7	68 ± 10	>100
5a	64 ± 11	63 ± 7	27 ±2	63 ± 6
5b	56 ± 16	33 ± 4	24 ± 2	62 ± 3
Cisplatin	21 ± 3	9.5 ± 1.5	29 ± 4	25± 5

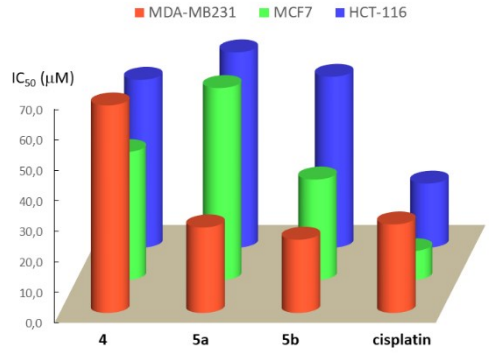

Figure 11. Comparative plot of the IC_{50} values (μM) of the new compounds **2**, **4**, **5a** and **5b** against the cisplatin-resistant colon cancer cell line (HCT-116) and the two breast cancer cell lines (MCF7 and MDA-MB231) used in this work. For comparison data obtained for cisplatin under identical experimental conditions are also included.

The comparison of the IC_{50} values obtained in the HCT-116 cell line reveals that the ferrocenylsulfonylhydrazine (**2**) does not exhibit any significant activity, but the sulfonylhydrazones **4**, **5a** and **5b**, had moderate inhibitory growth potency (IC_{50} in the range 55 μM- 65μM) but, clearly lower than those of cisplatin (IC_{50} = 21 ± 3 μM) and the aldimine [Fe(η^5-C_5H_5)(η^5-C_5H_4)-N=CH-(η^5-C_5H_4)Re(CO)$_3$] shown in **Fig. 2**, **D** (IC_{50} = 7.8 ± 3.3 μM [35a]) in the HCT-116 colon cancer cell line. These findings suggest that the incorporation of the –SO_2-NH- unit between the (C_5H_4) ring of the ferrocenyl unit and the imine carbon of **D**, reduces the potency of the compound in this cell line. However, it should be noted that the new cyrhetrenyl and cymantrenyl derivatives (**5a** and **5b**, respectively) are more active than the 2,4-dihydro-1H-3,1-benzoxazines (**E,F**) (**Fig.2**) with the [M(η^5-C_5H_4)(CO)$_3$] (M = Re or Mn) arrays units on position 2 (IC_{50} > 100 μM)[35b]. Therefore, the replacement of the bicyclic system by the –CH=N-NH-SO_2R unit (R = ferrocenyl unit) produces a significant enhancement of their inhibitory growth activity in the HCT-116 cell line.

In view of these results in the next stage we focused our attention on two markedly different breast cancer cell lines: the MCF7 and the MDA-MB231 breast cell lines that belong to the *Luminal A* and *claudin-low* subtypes, respectively).[58]

As shown in **Table 4** and **Figure 11**, the results obtained in the MCF7 cancer cell line show that their inhibitory growth potency increases according to the sequence: **2** << **5a** < **4** < **5b** < cisplatin. Similary to what happened in the HCT116 and MCF7 cell lines, the sulfonylhydrazine derivative (**2**) did not show any significant activity in the triple negative (ER, PR and no HER2 over expression) MDA-MB231 breast cancer cell line and the homodimetallic compound (**4**) exhibited moderate activity.

More interesting were the results obtained for **5a** and **5b** whose inhibitory growth effect was similar to that of cisplatin (the differences between their IC_{50} values are minimal) On these basis, compounds **5a** and **5b** are particularly attractive because they do not contain Pt(II) and consequently might not produce the typical and undesirable side effects of conventional Pt(II)-based drugs.

In view of this and in order to get further information about their effect on normal cancer cell lines, a parallel study was carried out on normal and non-tumoural human skin fibroblast BJ cell line. The results (**Table 4** and **Fig. S17**) show that the new compounds **2-5** are in general less toxic than cisplatin in the BJ cell line under identical experimental conditions and their cytotoxicity increases according to the sequence: **2** ≈ **4** < **5a** ≈ **5b** < cisplatin.

Another important parameter in novel anticancer drugs discovery is the selectivity index (SI)[§§]. Compounds **5a** and **5b**, that showed an inhibitory growth effect on the MB-MDA231 cell line similar to that of cisplatin, exhibited lower toxicity in the normal and non-tumoural cell lines. The SI values in the MB-MDA231 cell line for cisplatin in the MB-MDA231 cell line (SI = 0.9) is smaller than those of compounds **5a** and **5b** (2.3 and 2.6, respectively) under identical conditions. It is well-known that high SI values (> 2) of a compound gives selective toxicity to cancer cells. Although, the inhibitory growth potency of **5a** and **5b** is not spectacular, their selectivity indexes, enhance the potential interest of compounds **5a** and **5b**.

DOI: 10.1039/D0DT01756F

Experimental

Materials and methods

Unless otherwise noted, all manipulations were carried out under an N_2 atmosphere using Schlenk techniques. Ferrocenecarboxaldehyde (98%) and hydrazine (solution 1.0 M in THF) were obtained from Aldrich and used as received. Compound [Fe(η^5-C_5H_4){(η^5-C_5H_4)-S(O)$_2$-Cl}][41] and the aldehydes [M{(η^5-C_5H_4CHO)}(CO)$_3$] (M = Re or Mn) were prepared as described previously[59]. Solvents were obtained commercially and purified using standard methods[60].

Infrared spectra were recorded in solution (CH_2Cl_2) or as KBr disks in the range 4000-400 cm^{-1} on a Jasco FT-IR 4600 spectrophotometer.

Elemental analyses were performed with a Perkin–Elmer PE 2400 elemental analyzer. High resolution mass spectra (HRMS) were registred at the Servei de *Espectrometría de Masses* (Univ. Barcelona) with a LC/MSD-TOF Agilent Technologies instrument and electron impact (EI) mass spectra were obtained on a Shimadzu GC-MS spectrometer (70 eV) at the Laboratorio de Servicios Analíticos, (Pontificia Universidad Católica de Valparaíso). ^{1}H and ^{13}C{^{1}H} NMR spectra of the new products in $CDCl_3$ (for **2**) and in acetone-d_6 (for **3**, **4**, **5a** and **5b**) were recorded at 298 K on a Mercury 400 MHz instrument or on a Bruker AVANCE 500 MHz spectrometer. Chemical shifts (δ) that were internally referenced using the residual solvent signals, are given in ppm and the coupling constants (*J*) in Hz. NMR data in $CDCl_3$ for **2** or in acetone–d_6 for **4**, **5a** and **5b** are presented in the characterization section of the corresponding compound. The assignment of the resonances refers to the labelling patterns shown in **Scheme 1** and the abbreviations for the multiplicities of the signals are: s (singlet), d (doublet) and t (triplet) and br (broad signal). ^{1}H-NMR spectra of compounds **2-5** in CD_3CN registered at 298 K are presented in the **Figs. S4-S7**. Finally, ^{1}H-NMR spectra of freshly prepared solutions of the dimetallic compounds **4**, **5a** and **5b** in DMSO-d_6 and in a DMSO-d_6: D_2O (1: 1) mixture and after different periods of storage (*t*) at 298 K are included in the *Supplementary materials* (**Figs. S8-S13**).

Synthesis of ferrocenyl sulfonyl hydrazide [Fe(η^5-C_5H_5){(η^5-C_5H_4)-S(O)$_2$-NH-NH$_2$}] (2). A Schlenk tube was charged with [Fe(η^5-C_5H_5){(η^5-C_5H_4)-S(O)$_2$-Cl}] (1.43 g, 5.0 mmol), 5 mL of dry THF at -10 °C, and stirred for 5 min. Then, 10 mL (10.0 mmol) of hydrazine (1.0 M in THF) were added dropwise. The reaction mixture was stirred vigorously for 24 h at room temperature. Finally, the solvent was removed by reduced pressure giving a yellow solid that was collected and dried in vacuum. Yield: 80% (1.12 g, 4.0 mmol). *Characterization data:* IR data (selected bands) (KBr, cm^{-1}): 3361 [ν(N-H)], 3276 [ν(N-H)], 3242 [ν(N-H)], 1345 [ν_a(S=O)] and 1148 [ν_s(S=O)]. ^{1}H-NMR data ($CDCl_3$): δ_{1H} = 3.62 (s, 2H, -NH$_2$), 4.46 (s, 5H, Cp), 4.48 (t, 2H, ^3J = 2.3, H^3 and H^4), 4.72 (t, 2H, ^3J = 2.3, H^2 and H^5), 5.40 (s, 1H, -NH). ^{13}C{^{1}H}-NMR data ($CDCl_3$): δ_{13C} = 69.6 (C^2 and C^5), 70.9 (Cp), 71.3 (C^3 and C^4) and 82.9 (C^1).¥ Mass spectrum: HRMS (*m/z*): 281.0035, calc. for {[M]+H}$^+$ ($C_{10}H_{13}FeN_2O_2S$): 281.0042 and EIMS *m/z*: 280 [M$^+$]. Anal. (%) Calc. for $C_{10}H_{12}FeN_2O_2S$: C, 42.88; H, 4.32 and N, 10.00; found: C, 42.82; H, 4.30; N, 10.12.

***Synthesis of [(η^5-C_5H_5)Fe{(η^5-C_5H_4)-S(O)$_2$-NH-N=C(CH$_3$)$_2$}]* (3).** In a beaker of 10 mL with 50 mg of compound **2** (0.18 mmol) was added 5 mL of acetone (68.00 mmol), the mixture was allowed to stand until complete evaporation of the solvent. The resulting yellow solid was analysed without further purification giving compound **3** in pure form. [Yield: 96% (55.4 mg, 0.17 mmol). IR data (selected bands) (KBr, cm^{-1}): 3211 [ν(N-H)], 1637 [ν(-C=N-)], 1342 [ν_a(S=O)] and 1145 [ν_s(S=O)]. Mass spectrum: HRMS (*m/z*): 321.0353, calc. for {[M]+H}$^+$ ($C_{13}H_{17}FeN_2O_2S$): 321.0355.

General procedure for the synthesis of the homo-, and hetero-bimetallic hydrazone derivatives [Fe(η^5-C_5H_5){[(η^5-C_5H_4)-S(O)$_2$-NH-N=CH-(η^5-C_5H_4)]Fe(η^5-C_5H_5)}] (4) and [Fe(η^5-C_5H_5){[(η^5-C_5H_4)-S(O)$_2$-NH-N=CH-(η^5-C_5H_4)]M(CO)$_3$}] with M = Re (5a) or Mn (5b).

A Schlenk tube was charged with a magnetic stir bar, ferrocenyl-sulfonyl hydrazide **2** (1.0 mmol), 12 mL of water and three drops of HCl (32%). The resulting suspension was stirred for 5 min at room temperature. Then, 1.0 mmol of [Fe(η^5-C_5H_5){(η^5-C_5H_4)-CHO}] for **4** or the appropriate organometallic aldehyde [M{(η^5-C_5H_4)-CHO)}(CO)$_3$], M = Re (for **5a**) or Mn (for **5b**) was added. The resulting mixture was stirred for 18 h at room temperature. The orange (for **4**) or whitish (for **5a** and **5b**) solid formed was filtered off, washed with water (2 × 10 mL) and dried under vacuum. The heterodimetallic compounds **5a** and **5b** were later on treated with an acetone:hexane (1:5) mixture and the resulting solutions were stored at -18 °C. After one day the crystals formed were collected and dried. Yields: 80% (380.9 mg, 0.8 mmol) for **4**, 90% (562.9 mg; 0.9 mmol) for **5a** and 90% (444.7 mg; 0.9 mmol) for **5b**.

Characterization data for [Fe(η^5-C_5H_5){[(η^5-C_5H_4)-S(O)$_2$-NH-N=C(H)-(η^5-C_5H_4)]Fe(η^5-C_5H_5)}] **(4)**. IR (KBr, cm^{-1}): 3106 [ν(N-H)], 1600 [ν(-C=N-)], 1350 [ν_a(S=O)] and 1139 [ν_s(S=O)]. ^{1}H-NMR data (acetone-d_6): δ_{1H} = 4.07 (s, 5H, *Cp*); 4.35 (s, 2H, H^3 and H^4); 4.42 (s, 5H, Cp); 4.49 (s, 2H, H^2 and H^5); 4.58 (s, 2H, H^2 and H^5); 4.72 (s, 2H, H^3 and H^4); 7.81 (s, 1H, -CH=N) and 9.28 (s, 1H, NH). ^{13}C{^{1}H}-NMR data (acetone-d_6): δ_{13C} = 67.6 (C^3 and C^4); 69.1 (C^2 and C^5); 69.3 (C^2 and C^5); 69.9 (C^3 and C^4); 70.6 (Cp); 70.8 (*Cp*); 78.9 (C^1); 87.3 (C^1) and 147.9 (-CH=N). Mass spectrum: HRMS (*m/z*): 477.0008, calc. for {[M]+H}$^+$ ($C_{21}H_{21}Fe_2N_2O_2S$): 477.0018 and EIMS *m/z*: 476 [M$^+$]. Anal. (%) Calc. for $C_{21}H_{20}Fe_2N_2O_2S$: C, 52.97; H, 4.23 and N, 5.88; found: C, 53.16; H, 4.30 and N, 5.97.

Characterization data for [Fe(η^5-C_5H_5){[(η^5-C_5H_4)-S(O)$_2$-NH-N=CH-(η^5-C_5H_4)]Re(CO)$_3$}] (**5a**). IR data (selected bands) (KBr, cm^{-1}): 3146 [ν(N-H)], 2020 [ν(CO)], 1932 [ν(CO)], 1590 [ν(-C=N-)], 1354 [ν_a(S=O)] and 1193 [ν_s(S=O)]. IR-data (in CH_2Cl_2, cm^{-1}): 2025 [ν(CO)], 1943 [ν(CO)], and 1605 [ν(-C=N-)]. ^{1}H-NMR data (acetone-d_6): δ_{1H} = 4.40 (s, 5H, Cp), 4.46 (t, 2H, ^3J = 1.9, H^2 and H^5), 4.66 (t, 2H, ^3J = 1.9, H^3 and H^4), 5.64 (t, 2H, ^3J = 2.0, H^3 and H^4), 6.07 (t, 2H, ^3J = 2.0, H^2 and H^5), 7.71 (s, 1H, -CH=N) and 9.83 (s, 1H, NH). ^{13}C{^{1}H}-NMR data (acetone-d_6): δ_{13C} = 68.9 (C^2 and

C^5); 70.4 (Cp); 70.6 (C^3 and C^4); 85.0 (C^3 and C^4); 85.3 (C^2 and C^5); 86.9 (C^1); 99.1 (C^1); 139.1 (-CH=N); 193.7 (CO). Mass spectrum: HRMS (*m/z*): 626.9680, calc. for $\{[M]+H\}^+$ ($C_{19}H_{16}FeN_2O_5ReS$): 626.9680 and EIMS (based on ^{187}Re) *m/z*: 626 [M^+] and 542 [M^+-3CO]. Anal. (%) Calc. for $C_{19}H_{15}FeN_2O_5ReS$: C, 36.49; H, 2.42 and N, 4.48; found: C, 36.54; H, 2.44 and N, 4.58.

Characterization data for $[(\eta^5\text{-}C_5H_5)Fe\{[(\eta^5\text{-}C_5H_4)\text{-}S(O)_2\text{-}NH\text{-}N{=}CH\text{-}(\eta^5\text{-}C_5H_4)]Mn(CO)_3\}]$ **(5b)**. IR data (selected bands) (in KBr, cm^{-1}): 3145 [ν(N-H)], 2019 [ν(CO)], 1932 [ν(CO)], 1595 [ν(-C=N-)], 1354 [ν_a(S=O)], and 1194 [ν_s(S=O)]. IR-data (in CH_2Cl_2, cm^{-1}): 2025 [ν(CO)], 1943 [ν(CO)] and 1605 [ν(-C=N-)]. ^{1}H-NMR data (acetone-d_6): δ_{1H}= 4.40 (s, 5H, Cp), 4.45 (s, 2H, H^2 and H^5), 4.67 (t, 2H, H^3 and H^4), 5.02 (s, 2H, H^3 and H^4), 5.44 (s, 2H, H^2 and H^5), 7.64 (s, 1H, -CH=N) and 9.83 (s, 1H, NH). ^{13}C{^{1}H}-NMR data (acetone-d_6): δ_{13C} = 69.1 (C^2 and C^5); 70.4 (Cp); 70.6 (C^3 and C^4); 83.1 (C^3 and C^4); 83.9 (C^2 and C^5); 86.8 (C^1); 95.1 (C^1) and 140.2 (-CH=N-)&. Mass spectrum: HRMS (*m/z*): 494.9500, calc. for $\{[M]+H\}^+$ ($C_{19}H_{16}FeN_2O_5MnS$): 494.9505 and EIMS (based on ^{55}Mn) *m/z*: 494, [M^+] and 410 [M^+-3CO]. Anal. (%) Calc. for $C_{19}H_{15}FeN_2O_5MnS$: C, 46.18; H, 3.06 and N, 5.67; found: C, 46.28; H, 3.09 and N, 5.76.

X-ray crystal structure determinations.

The crystals of **3, 5a** and **5b** were carefully chosen using a stereo zoom microscope supported by a rotatable polarizing stage. The data were collected at room temperature on a Bruker APEX II CCD Duo equipped with a Mo Incoatec microsource (0.71073 Å). The crystals were glued to a thin glass fibre using inert oil and mounted on the diffractometer. The intensity data were processed using a Bruker suite of data processing programs[61] and absorption corrections were applied using SADABS (Siemens Industrial Automation, Inc., 1996). The crystal structure was solved by the charge flipping method using SUPERFLIP[62] and the data were refined by full matrix least-squares refinement on F^2 with anisotropic displacement parameters for non-H atoms using CRYSTALS[63].

CCDC-2003815 (for **3**), 2003816 (for **5a**) and 2003817 (for **5b**) contain the supplementary crystallographic data for this paper. These data can be obtained free of charge from *The Cambridge Crystallographic Data Centre* via www.ccdc.cam.ac.uk/data_request/cif.

Electrochemical studies Cyclic voltammetric (CV) studies were carried out at room temperature using a potentiostat (model PGSTAT302N Metrohm Autolab) in a three-electrode cell. Each complex was dissolved in acetonitrile containing 0.1 mol/L Tetrabutylammonium hexafluorophosphate, $(Bu_4N)[PF_6]$, as supporting electrolyte to give 10^{-3} mol/L final concentration. A platinum 2 mm working electrode, and platinum coil counter electrode was used. The reference electrode contained a silver wire with 10 mM silver nitrate in $(Bu_4N)[PF_6]$ electrolyte solution.

The working electrode was polished with 0.3 and 0.05 µm alumina slurries, rinsed with distilled water (18 MΩ cm) and acetone and dried prior to use. All electrolyte solutions were thoroughly pre-purged using purified nitrogen gas before use. The measurements were carried out at 0.1 V/s scan rate. The ferrocene/ferricinium (Fc/Fc^+) couple served as internal reference and appeared at +86 mV (vs Ag/Ag^+) for each experiment.

Computational studies

DFT calculations have been performed using Q-Chem 5.1[55] included in Spartan 18[56], using the B3LYP[57] functional. The basis set has been chosen as follows: 6-31G*, included polarization for non-hydrogen atoms[64-66], for H, C, N, O, S, Fe and Mn; and LANL2DZ[67], for Re. Geometries have been optimized without imposing symmetry restrictions, on the most stable conformers found using the augmented MMFF94 method[68], implemented in Spartan 18.

Biological Studies

Cell culture. Colon adenocarcinoma (HCT116) cells (from the *American Type Culture Collection*) and breast cancer (MCF7 and MDA-MB231) cells (from *European Collection of Cell Cultures*, ECACC) were used for all the experiments. Cells were grown as a monolayer culture in DMEM-high glucose (Sigma, D5796) in the presence of 10 % heat-inactivated fetal calf serum and 0.1 % streptomycin/penicillin in standard culture conditions. The human skin fibroblast cell line BJ was cultured in MEM (Sigma, M2279) in the presence of 10 % FBS, 4 mM glutamine, and 0.5 % streptomycin/penicillin. All the cells were incubated under standard conditions (humidified air with 5 % CO_2 at 37 °C). The cells were passaged at 90 % confluence by washing once with cation-free HBSS followed by a 3 min incubation with trypsin ([0.5 µg/mL]/EDTA [0.2 µg/ mL]) (Gibco-BRL, 15400054) solution in HBSS at 37 °C, and transferred to its medium. Prior to seeding at a defined cell concentration, the cells were recovered from the medium by centrifugation and counted.

Cell viability assays. For these studies, compounds were dissolved in 100 % DMSO at 50 mM as stock solution; then, consecutive dilutions have been done in DMSO (1:1) (in this way DMSO concentration in cell media was always the same); followed by 1:500 dilutions of the solutions of compounds on cell media. The assay was carried out as described by Givens et al.[69], in brief, MDA-MB231 and MCF7 cells were plated at 5000 cells/well or 10,000 cells/well respectively, in 100 µL media in tissue culture 96 well plates (Cultek). BJ cells were plated at 2500 cells per well. After 24h, medium was replaced by 100 µL/well of serial dilution of drugs. Each point concentration was run in triplicate. Reagent blanks, containing media plus colorimetric reagent without cells were run on each plate. Blank values were subtracted from test values and were routinely 5–10 % of uninhibited control values. Plates were incubated for 72 h. Hexosamidase activity was measured according to the following protocol: the media containing the cells was removed and cells were washed once with phosphate buffer saline (PBS) 60µL of substrate solution (p-nitrophenol-N-acetyl-β-D-glucosamide 7.5 mM [Sigma N9376], sodium citrate 0.1 M, pH = 5.0, 0.25 % Triton X-100) was added to each well and incubated

View Article Online
DOI: 10.1039/D0DT01756F

at 37 °C for 1–2 h; after this incubation time, a bright yellow colour appeared; then, plates could be developed by adding 90 µL of developer solution (Glycine 50 mM, pH = 10.4; EDTA 5 mM), and absorbance was recorded at 410 nm.

Conclusions

Here we have presented the synthesis and characterization of the novel ferrocenyl sulfonyl hydrazide [Fe(η^5-C_5H_5){(η^5-C_5H_4)-$S(O)_2$-NH-NH_2}] (**2**). Its high proclivity to react with aldehydes and ketones has allowed us to obtain [Fe(η^5-C_5H_5){(η^5-C_5H_4)-$S(O)_2$-NH-N=CMe_2}] (**3**) and the dimetallic derivatives [Fe(η^5-C_5H_5){[(η^5-C_5H_4)-$S(O)_2$-NH-N=CH-(η^5-C_5H_4)]Fe(η^5-C_5H_5)}] (**4**) and [Fe(η^5-C_5H_5){[(η^5-C_5H_4)-$S(O)_2$-NH-N=CH-(η^5-C_5H_4)]M$(CO)_3$}] with M = Re (**5a**) or Mn (**5b**). The X-ray crystal structures of compounds **3**, **5a** and **5b** confirmed the proposed formulae, revealed the existence of intermolecular contacts involving the SO_2 and -NH- units and a nearly orthogonal orientation of the C_5H_4 ring of the ferrocenyl unit and the plane formed by the set of atoms defining the hydrazine backbone. In compounds **5a** and **5b**, hydrazine unit adopts the *E*- form but despite they differ exclusively in the nature of the metal ion Re (in **5a**) or Mn (in **5b**) their crystal architectures are markedly different.

We have also proved that the dimetallic compounds **4**, **5a** and **5b**, exhibit high stability in solution and also in the solid state, while compounds **2** and **3** are less stable. The hydrazine derivative **2**, exhibits high reactivity in front of aldehydes and ketones, and compound **3**, that tends to hydrolyze easily.

Comparative experimental studies on their electrochemical properties and absorption spectra have provided conclusive evidences of the effects produced by the substituents attached to the "[Fe(η^5-C_5H_5){[(η^5-C_5H_4)-$S(O)_2$-NH-" core on their electrochemical and spectroscopic properties.

Theoretical studies based on DFT and TD-DFT methodologies for the new compounds have allowed us to understand results obtained from the electrochemical studies and UV-vis. spectra. Compound **2** and the hydrazine derivatives **3**, **5a** and **5b** are less prone to undergo the first oxidation process than **4**. The MO calculations reveal that the HOMO of **2**, **3**, **5a** and **5b**, is mainly centred on the ferrocenyl unit; while for the homodimetallic derivative the main contributions arise from the other ferrocenyl unit. The first oxidation requires the removal of the electron in the HOMO of **4** which is markedly different from those of **2**, **3**, **5a** and **5b**.

The absorption spectra of CH_2Cl_2 solutions of compounds **2-4**, **5a** and **5b** at 298 K are complex and show broad bands with low resolution. The computational studies reveal the existence of numerous monoelectronic transitions in a narrow range of energy, that may cause the overlapping of bands

In vitro studies on the cytotoxic activity of [Fe(η^5-C_5H_5){(η^5-C_5H_4)-$S(O)_2$-NH-NH_2}] (**2**) and the dimetallic compounds **4**, **5a** and **5b** in the cancer cell lines (HCT116, MCF7 and MB-MDA-231) and in normal and non-tumoural human skin fibroblasts BJ cell line show that: a) compound **2** did not show any relevant activity in any of the cell lines selected for this study; b) the dimetallic sulfonylhydrazones (**4**, **5a** and **5b**) exhibit moderate inhibitory growth effect in the HCT116 and MCF7 cell lines, their potency is clearly smaller than that of cisplatin, but they are less toxic than the reference drug in normal and non-tumoural cell lines, and c) in the triple negative MB-MDA231 cell line the di(Ferrocenyl) derivative **4** shows moderate activity, but the heterodimetallic compounds that arise from **4** by replacement of the Fe(η^5-C_5H_5)(η^5-C_5H_4) group by the [M{(η^5-C_5H_4)}$(CO)_3$] (M = Re or Mn) units enhances the inhibitory growth effect. Compounds **5a** and **5b** (IC_{50} = 27 ± 2 µM and 24 ± 2 µM, respectively) exhibit a cytotoxic effect on the MB-MDA231 cells similar to that of cisplatin (29 ± 4 µM) under identical experimental conditions, but they are less potent than the imine **D**, shown in **fig. 2** (IC_{50} = 7.4 ± 1.5 µM[35a]). However, the low toxicity of **5a** and **5b** in the normal and non-tumoural BJ cell line, suggests that these compounds exhibit selective toxicity to the MDA-MB231 cancer cells, that under hypoxic conditions express high hCA-IX levels[70].

Among the new compounds presented here, the dimetallic derivatives [Fe(η^5-C_5H_5){(η^5-C_5H_4)-$S(O)_2$-NH-N=CHR) }] with R = ferrocenyl, (**4**) cyrhetrenyl (**5a**) or cymantrenyl (**5b**), with high stability and low toxicity in normal cell lines are excellent candidates for further studies on: a) their effect on a wider panel of cell lines, b) their potential as hCA inhibitors, c) the mechanism of action of **5a** and **5b**, d) other biological activities (i.e. antibacterial, antifungal, etc.), that maybe relevant in new drug design and development.

Authors information

Corresponding Authors *E-mail: rarancibia@udec.cl; conchi.lopez@qi.ub.es

ORCID Yosselin Huentupil: 0000-0001-5453-0232; Patricio Chung: 0000-0003-02277-2629; Néstor Novoa: 0000-0002-7167-2694; Rodrigo Arancibia: 0000-0003-0689-9080; Pascal Roussel: 0000-0001-7243-7293; Juan Oyarzo: 0000-0002-1778-3051; A. Hugo Klahn: 0000-0003-3979-2693; Carlos Silva: 0000-0001-5344-042X; Ramon Messeguer: 0000-0003-1913-7624; Ramón Bosque: 0000-0002-4796-5673; Concepción López: 0000-0001-7433-9582.

Conflicts of interest: There are no conflicts to declare.

Acknowledgements

R.A. acknowledges FONDECYT-Chile (Project 1190327); J.O. is grateful to D.I.-PUCV for postdoctoral position (Project 37.0/2019); R.B and C.L. are also grateful to the *Ministerio de Economía y Competitividad* of Spain for financial support [Grant n. CTQ-2015-65040P (subprogram BQU)].

Notes and references

‡Phase I finished and now entering in phase II.

‡‡Crystal data for compound **3**: $C_{13}H_{16}FeN_2O_2S$, FW = 320.20, *Monoclinic*, space group = *C2/c*, *a* = 20.8459(10) Å, *b* = 9.8908(5)

View Article Online DOI: 10.1039/D0DT01750F

Å, c = 13.3379(7) Å, $\alpha = \gamma = 90°$ and $\beta = 95.843(3)°$, V = 2735.8(2) Å^3, Z = 8 and $D_{calc.}$ = 1.555 Mg × m^{-3} (See also **Table S1**).

§ Crystal data for compound **5a**: $C_{19}H_{15}FeN_2O_5ReS$, FW= 625.44, *Monoclinic*, space group = $P2_1/n$, a = 12.6127(8) Å, b = 7.7038(5) Å, c = 22.053(15) Å, $\alpha = \gamma = 90°$ and $\beta = 99.323(2)°$, V = 2109.9(2) Å^3, Z = 4 and $D_{calc.}$ = 1.969 Mg×m^{-3}. For compound **5b**: $C_{19}H_{15}FeMnN_2O_5S$, FW = 494.18, *Triclinic*, space group = *P-1*, a = 7.1339(3) Å, b = 15.3593(6) Å, c = 18.4395(7) Å, α = 80.8480(19)°, β = 84.4154(17)° and γ = 81.2946(17)° V = 1996.19(14) Å^3, Z = 4 and $D_{calc.}$ = 1.669 Mg × m^{-3} (See also **Table S1**).

Comparison of the ^{1}H NMR spectra registered and those of the initial compounds and the precursors, reveals that the signals due to the minor species are coincident with those of the organometallic aldehydes used as precusors.

ϒ It should be noted that in the Uv-vis. spectra of **5a** no evidences of any absorption band, or even a shoulder, at ca. 261 nm were detected, this is consistent with the results obtained from the computational studies, because no monoelectronic transition in this range was detected.

§§ *Selectivity index* (SI) = [IC_{50} in the normal and non-tumoural cell line]/[IC_{50} in a specific cancer cell line].

¥ As a consequence of the high proclivity of compound **2** to react with acetone to give **3**, even at room temperature, the solvent used for the characterization of [Fe(η^5-C_5H_5){(η^5-C_5H_4)-S(O)$_2$-NH-NH_2}] (**2**) in solution was $CDCl_3$ instead of acetone–d_6.

& The signals due to the ^{13}C-nuclei of the CO ligands were not detected.

1 https://www.cancer.org/research/cancer-facts-statistics/all-cancer-facts-figures/cancer-facts-figures-2020.html

2 (a) F. Bray, J. Ferlay, I. Soerjomataram, R. L. Siegel, L. A. Torre and A. Jemal, CA *Cancer J. Clinic*. 2018, **68**, 394–424; (b) https://gco.iarc.fr/tomorrow/home, (assessed on March 2019).

3 https://www.persistencemarketresearch.com/market-research/anticancer-drugs-market.

4 (a) S. Mukherjee, S. Sanyal and S. Chadra (eds.), *Rediscovering Cancer from Mechanism to Therapy*, CCD Press 2018; (b) D. Rosenblum, N. Joshi, W. Tao, J. M. Karp and D. Peer, *Nat. Commun.* 2018, **9**, 1410.

5 (a) C. Viegas-Junior, A. Danuello, V. da Silva Bolzani, E. J. Barreiro and C. A. Fraga, *Curr. Med. Chem*., 2007, **14**, 1829–1852; (b) M. Decker, *Design of Hybrid Molecules for Drug Development,* 2017, Elsevier; (c) M. de Olivera Pedrosa, R. M. Duarte da Cruz, J. de Oliveira Viana, R. O. de Moura, H. M. Ishiki, J. M. Barbosa Filho, M. F. Diniz, M. T. Scotti, L. Scotti and F. J. Bezerra Mendonca, *Curr. Top. Med. Chem.*, 2017, **17**, 1044–1079; (d) S. M. Shaveta and P. Singh, *Eur. J. Med. Chem.*, 2016, **124**, 500–536.

6 Selected articles on the relevance of multitargeted products in new drugs design: (a) E. Proschak, H. Stark and D. Merk, *J. Med. Chem.*, 2019, **62**, 420–444; (b) M. L. Bolognesi, *ACS Med. Chem. Lett.*, 2019, **10**, 273–275; (c) R. R. Ramsay, M. R. Popovic-Nikolic, K. Nikolic, E. Uliassi and M. L. Bolognesi, *Clin. Transl. Med.*, 2018, **7**, 3; (d) J-J. Lu, W. Pan, Y-J. Hu and W-T. Wang, *PLoS ONE,* 2012, **7**, e40262.

7 Selected papers on multitarget anticancer drugs: (a) X. Ke and L. Shen, *Front. Lab. Med.*, 2017, **1**, 69–75; (b) E. Kucuksayan and T. Ozben, *Curr. Top Med. Chem.*, 2017, **17**, 907–918; (c) M. Zajac, I. Muszalska and A. Jelinska, *Curr. Med. Chem.*, 2016, **23**, 4176–4220; (d) N. M. Raghavendra, D. Pingili, S. Kadasi, A. Mettu and S. V. U. M. Prasad*, Eur. J. Med. Chem.*, 2018, **143**, 1277–1300; (e) J.-N. Chen, *Curr. Top. Med. Chem.*, 2017, **17**, 3081–3083; (f) W. Zheng, Y. Zhao, Q. Luo, Y. Zhang, K. Wu and F. Wang, *Curr. Top. Med. Chem.*, 2017, **17**, 3084–3098; (g) Z-F. Chen, C. Orvig and H. Liang, *Curr. Top. Med. Chem.*, 2017, **17**, 3131–3145; (h) L. Xie and P. E. Bourne, *Front. Pharmacol.*, 2015, **6**, 209; (i) M. L. Bolognesi, A. Cavalli, *ChemMedChem,* 2016, **11**, 1190–1192; (j) S. Sestito, M. Runfola, M. Tonelli, G. Chiellini and S. Raposelli, *Front. Pharmacol.*, 2018, **9**, 874.

8 A. Pawełczyk, K. Sowa-Kasprzak, D. Olender and L. Zaprutko, *Int. J. Mol. Sci.*, 2018, **19**, 1104.

9 See for instance: (a) P. Vaupel and A. Mayer, *Cancer Metastasis Rev.*, 2007, **26**, 225–239; (b) I. Daskalaki, I. Gkikas and N. Tavernarakis, *Front. Cell Dev. Biol.*, 2018, **6**, 104; (c) K. Graham and E. Unger, *Int. J. Nanomedicine*, 2018, **13**, 6049–6058; (d) A. Challapalli, L. Carroll, and E. O. Aboagye, *Clin. Transl. Imaging*, 2017, **5**, 225–253; (e) B. Muz, P. de la Puente, F. Azab and A. K. Azab, *Hypoxia (Auckl)*, 2015, **3**, 83–92; (f) D. M. Gilkes, G. L. Semenza and D. Wirtz, *Nat. Rev. Cancer.*, 2014, ***14***, 430–439; (g) P. Vaupel and A. Mayer, *Adv. Exp. Med. Biol.*, 2014, **812**, 19–24.

10 (a) C. T. Supuran and A. Nocentini *Carbonic Anhydrases Biochemistry and Pharmacology of an Evergreen Pharmaceutical Target*, 1st Ed., Academic press, 2019. (b) C. T. Supuran, Metabolites, 2018, **8**, 25; (c) C. T. Supuran, *Expert Opin. Investig. Drugs*, 2018, **27**, 963–970.

11 (a) S. Singh, C. L. Lomelino, M. Y. Mboge, S. C. Frost, and R. McKenna, *Molecules*, 2018, **23**, 1045; (b) M. A. Ilies and J.-Y Winum, *Carbonic Anhydrases*, eds. C. T. Supuran and A. Nocentini, 2019, Chapter 16, 331–365; (c) S. Pastorekova, M. Barathova, J. Kopacek and J. Pastorek, *Drug design of Zinc-Enzyme Inhibitors: Functional, Structural, and Disease Applications*, eds. C. T. Supuran and J.-Y Winum, 2009, chapter 8, 193; (d) J. Kazokaite, A. Aspatwar, S. Parkkila and D. Matulis, *PeerJ,* 2017, **5**, e-4068.

12 R. Lavanya, *Int. J. Pharm. Sci. Inv.*, 2017, **6**, 01–03.

13 For a general overview on sulfonamides and their derivatives in drugs design see for instance (a) I. Gulçin and P. Taslimi, *Expert Opin. Ther. Patents*, 2018, **28**, 541–549; (b) M. Ferraroni, B. Cornelio, J. Sapi, C. T. Supuran and A. Scozzafava, *Inorg. Chim. Acta*, 2018, **470**, 128–132.

14 M. Y. Mboge, Z. Chen, A. Wolff, J. V. Mathias, C. Tu, K. D. Brown, M. Bozdag, F. Carta, C. T. Supuran, R. McKenna and S. C. Frost, *PLoS ONE,* 2018, 13, e0207417.

15 (a) F. Pacchiano, F. Carta, P. C. McDonald, Y. Lou, D. Vullo, A. Scozzafava, S. Dedhar and C. T. Supuran, *J. Med.Chem.*, 2011, **54**, 1898–1902;
(b) https://clinicaltrials.gov/ct2/show/NCT03450018.

16 E. Andreucci, J. Ruzzolini, S. Peppicelli, F. Bianchini, A. Laurenzana, F. Carta, C. T. Supuran and L. Calorini, *J. Enzyme Inhib. Med. Chem.,* 2019, **34**, 117–123.

17 I. Koyuncu, Y. Tuluce, H. S. Qadir, M. Durgun, and C. T. Supuran, *J. Enzyme Inhib. Med. Chem*., 2019, **34**, 703–711.

18 (a) E. S. Phillips, *Ferrocenes: Compounds, Properties, and Applications*, Nova Science Publishers, Hauppauge, 2011; (b) P. Stepnicka, *Ferrocenes: Ligands, Materials and Biomolecules*, Wiley-VCH, Weinheim, Germany, 2008.

19 G. Jaouen and P. J. Dyson, *in Comprehensive Organometallic Chemistry III*, eds. D. Mingos and R. Crabtree, Elsevier, Oxford, 2007, **12**, 445–464.

20 Selected contributions on the utility of organometallic compounds in cell imaging, as bioprobes, selective biosensors or as radiopharmaceuticals: (a) K. Lo, *Inorganic and Organometallic Transition Metal complexes with Biological Molecules and Living Cells*, Academic Press, 2016; (b) F. L. Thorp-Greenwood, R. G. Balasingham and M. P. Coogan, *J. Organomet. Chem*., 2012, **714**, 12–21; (c) A. Monney and M. Albrecht, *Coord. Chem. Rev*., 2013, **257**, 2420–2433; (d) I. S.

Butler, R. P. Kegne-Momo, G. Jaouen, C. Policar and A. Vessières, *Appl. Spectrosc. Rev.*, 2012, **47**, 531–549; (e) Z. Lam, K. V. Kong, M. Olivo and W. K. Leong, *Analyst*, 2016, **141**, 1569–1586.

21 (a) F. A. Larik, A. Saeed, T. A. Fattah, U. Muqadar and P. A. Channar, *Appl. Organomet. Chem*., 2017, **31**, e3664; (b) C. Ornelas, *New J. Chem*. 2011, **35**, 1973–1985; (c) D. Astruc, *Eur. J. Inorg. Chem.*, 2017, 6–29; (d) S. S. Braga and A. M. S. Silva, *Organometallics*, 2013, **32**, 5626–5639.

22 G. Jaouen and M. Salmain, *Bioorganometallic Chemistry: Applications in Drug Discovery, Biocatalysys and Imaging*, Wiley- VCH, Weinheim, 2015.

23 (a) G. Jaouen and N. Metzler-Nolte, *Topics in Organometallic Chemistry: Medicinal Organometallic Chemistr*y, Springer, Heildelberg, Germany, 2010, vol. *32*; (b) R. W. Brown and C. J. T. Hyland, *Med. Chem. Commun.,* 2015, **6**, 1230–1243; (c) M. P. Coogan, P. J. Dyson and M. Bochmann, *Organometallics*, 2012, **31**, 5671– 5672; (d) G. Gasser and N. Metzler-Nolte, *Curr. Opin. Chem. Biol.*, 2012, **16**, 84–91; (e) P. J. Dyson, *Chimia,* 2011, **65**, 730–733; (f) J. Yang, J. Zhao, Q. Cao, L. Hao, D. Zhou, Z. Gan, L. Ji and Z. Mao, *ACS Appl. Mater. Inter.*, 2017, **9**, 13900–13912; (g) F. Chen, I. Romero-Canelón, J. Soldevila-Barreda, J. Song, J. Coverdale, G. Clarkson, J. Kasparkova, A. Habtemariam, M. Wills, V. Brabec and P. J. Sadler, *Organometallics*, 2018, **37**, 1555–1566; (h) J. Zhao, D. Zhang, W.Hua, W. Li, G. Xu and S.Gou, *Organometallics* 2018, **37**, 3, 441–447.

24 (a) C. G. Hartinger, N. Metzler-Nolte and P. J. Dyson, *Organometallics*, 2012, **31**, 5677-5685; (b) P. Martins, M. Marques, L. Coito, A. J. Pombeiro, P. V. Baptista and A.R. Fernandes, *AntiCancer Agents Med. Chem.*, 2014, **14**, 1199–1212; (c) J. Hess, J. Keiser, and G. Gasser, *Future Med. Chem.*, 2015, **7**, 821–830; (d) M. B. Camarada, C. Echeverría and R. Ramírez-Tagle, *Med. Chem. Commun.*, 2016, **7**, 1307–1315; (e) N. Chavain and C. Biot, *Curr. Med. Chem*., 2010, **17**, 2729–2745; (f) G. Jaouen; A. Vessières and S. Top, *Chem. Soc. Rev*., 2015, **44**, 8802–8817; (g) J. Li, X. Liu, H. Zhang, X. Ge, Y. Tang, Z. Xu, L. Tian, X. Yuan, X. Mao and Z. Liu, *Inorg. Chem.*, 2019, **58**, 1710–1718; (h) X. Ge, S. Chen, X. Liu, Q. Wang, L. Gao, C. Zhao, L. Zhang, M. Shao, X. Yuan, L. Tian and Z. Liu, *Inorg. Chem.*, 2019, **58**, 14175–14184.

25 A selection of reviews on this topic: (a) M. M. Santos, P. Bastos, I. Catela, K. Zalewska and L. C. Branco, *Mini Rev. Med. Chem.*, 2017, **17**, 771-784; (b) D. Gambino and L. Otero, *Inorg. Chim. Acta*, 2018, **472**, 58–75; (c) A. Simonneau, F. L. Bideau, J.-H. Mirebeau, J. Marrot and G. Jaouen, *Curr. Top. Med. Chem.*, 2017, **17**, 2807–2819); (d) B. Albada and N. Metzler-Nolte, *Chem. Rev.*, 2016, **116**, 11797–11839; (e) S. S. Rodrigues, *Organometallic Compounds in Therapy: an expanding Horizon,* ed. H. F. Chin, Nova Science Publishers Inc, **2010**, pp. 293–308.

26 Selected articles: (a) C. López, R. Bosque, X. Solans and M. Font-Bardía, *New J. Chem.*, 1996, **20**, 1285-1292; (b) R. Bosque, C. López and J. Sales, *Inorg. Chim. Acta*, 1996, **244**, 141–145; (c) C. López, R. Bosque, S. Pérez, A. Roig, E. Molins, X. Solans, and M. Font-Fardía, *J. Organomet. Chem*., 2006, **691**, 475–484; (d) C. López, R. Bosque, X. Solans and M. Font-Bardia *J. Organomet. Chem.*, 1997, **547**, 309–317; (e) C. López and J. Granell, *J. Organomet. Chem.*, 1998, **555**, 211–225; (f) C. López, R. Bosque, X. Solans and M. Font-Bardía, *J. Organomet. Chem*., 1997, **539**, 99-107; (g) R. Bosque; C. López, X. Solans and M. Font-Bardia, *Organometallics*, 1999, **18**, 1267–1274.

27 (a) R. Arancibia, A. H. Klahn, G. E. Buono-Core, E. Gutierrez-Puebla, A. Monge, M. E: Medina, C. Olea-Azar, J. D. Maya and F. Godoy, *J. Organomet. Chem.*, 2011, **696**, 3238–3244; (b) R. Arancibia, A. H. Klahn, G. E. Bueno-Core, D. Contreras, G. Barriga, C. Olea-Azar, M. Lapier, J. D. Maya, A. Ibañez, M. T. Garland, *J. Organomet. Chem.*, 2013, **743**, 49–54.

28 R. Arancibia, F. Godoy, G. E. Buono-Core, A. H. Klahn, Gutierrez-Puebla and A. Monge, *Polyhedron*, 2008, **27**, 2421–2425.

29 R. Arancibia, F. Dubar, B. Pradines, I. Forfar, D. Dive, A. H. Klahn and C. Biot, *Bioorg. Med. Chem*., 2010, **18**, 8085–8091.

30 (a) C. Quintana, A. H. Klahn, V. Artigas, M. Fuentealba, C. Biot, I. Halloum, L. Kremer and R. Arancibia, *Inorg. Chem. Commun*., 2015, **55**, 48–50; (b) C. Echeverría, V. Romero, R. Arancibia, A. H. Klahn, I. Montorfano, R. Armisen, V. Borgna, F. Simon and R. Ramírez-Tagle, *Biometals*, 2016, **29**, 743–749.

31 Selected contributions on the anticancer activity of this type of compounds: (a) E. Guillén, A. González, C. López, P. K. Basu, A. Ghosh, M. Font-Bardía, C. Calvis and R. Messeguer, *Eur. J. Inorg. Chem*., 2015, **22**, 3781–3790; (b) E. Guillén, A. González, P. K. Basu, A. Ghosh, M. Font-Bardía, T. Calvet, C. Calvis, R. Messeguer and C. López, *J. Organomet. Chem.* 2017*,* **828***,* 122–132; (c) C. López, R. Bosque, M. Pujol, J. Simó, E. Sevilla, M. Font-Bardía, R. Messeguer and C. Calvis, *Inorganics*, 2014, ***2***, 620–640.

32 (a) D. Talancón, C. López, M. Font-Bardía, T. Calvet, J. Quirante, C. Calvis, R. Messeguer, R. Cortés, M. Cascante, L. Baldomà and J. Badía, *J. Inorg. Biochem.*, 2013, **118**, 1–12; (b) R. Cortés, M. Tarrado-Castellarnau, D. Talancón, C. López, W. Link, D. Ruíz, J. J. Centellas, J. Quirante and M. Cascante, *Metallomics*, 2014, **6**, 622–633.

33 (a) P. Toro, C. Suazo, A. Acuña, M. Fuentealba, V. Artigas, R. Arancibia, C. Olea-Azar, M. Moncada, S. Wilkinson and A. H. Klahn, *J. Organomet. Chem.*, 2018, **862**, 13–21; (b) J. Gómez, N. Leiva, R. Arancibia, J. Oyarzo, G. E. Buono-Core, A. H. Klahn, V. Artigas, M. Fuentealba, R. Bosque, G. Aullón, C. López, M. Font-Bardía and T. Calvet, *J. Organomet. Chem*., 2016, **819**, 129–137.

34 T. Cautivo, A. H. Klahn, F. Godoy, C. López, M. Font-Bardía, T. Calvet, E. Gutierrez-Puebla and A. Monge, *Organometallics*, 2011, **30**, 5578–558.

35 (a) J. Oyarzo, A. Acuña, H. Klahn, R. Arancibia, C. P. Silva, R. Bosque, C. López, M. Font-Bardía, C. Calvis and R. Messeguer, *Dalton Trans*., 2018, **47**, 1635–1649; (b) J. Oyarzo, R. Bosque, P. Toro, C. P. Silva, R. Arancibia, M. Font-Bardía, V. Artigas, C. Calvis, R. Messeguer, A. H. Klahn and C. López, *Dalton Trans*., 2019, **48**, 1023–1039.

36 G. R. Knox and P. L. Pauson, *J. Chem. Soc. Chem. Commun*., **1958**, 692–696.

37 K. Chanawanno, C. Holstrom, L. A. Crandall, H. Dodge, V. N. Nemykin, R. S. Herrick and C. J. Ziegler, *Dalton Trans.*, 2016, **45**, 14320–14326.

38 C. Quintana, G. Silva, A. H. Klahn, V. Artigas, M. Fuentealba, C. Biot, I. Halloum, L. Kremer, N. Novoa and R. Arancibia, *Polyhedron*, 2017, **134**, 166–172.

39 (a) A. Leonidova, C. Mari, C. Aebersold and G. Gasser, *Organometallics*, 2016, **35**, 851–854. (b) A. Leonidova and G. Gasser, *ACS Chem. Biol.*, 2014, **9**, 2180–2193.

40 (a) Y. Huentupil, L. Peña, N. Novoa, E. Berrino, R. Arancibia and C. T. Supuran, *J. Enzyme Inhib. Med. Chem.*, 2019, **34**, 451–458. (b) J. Brichet, R. Arancibia, E. Berrino and C. T. Supuran, *J. Enzyme Inhib. Med. Chem.*, 2020, **35**, 622-628.

41 G. Besenyei, L. Párkányi, S. Németh and L. Simándi, *J. Organomet. Chem*., 1998, **563**, 81–86.

42 H. Aslan and N. Karacan, *Med. Chem. Res.*, 2013, **22**, 1330–1338.

43 M. Movassaghi and O. K. Ahmad, *J. Org. Chem.*, 2007, **72**, 1838–1841; (b) C. R. Ojaja, W. H. Ojala, S. Y. Pennamon and W. B. Gleason, *Acta Cryst. Sect. C*, 1998, **C54**, 57–60.

44 C. Manzur, E. Baeza, L. Millan, M. Fuentealba, P. Hamon, J. Hamon, D. Boys and D. Carrillo, *J. Organomet. Chem.* 2000, **608**, 126–132.

45 *Cambridge Crystallographic Data Centre* (CCDC) https://www.ccdc.cam.ac.uk/ (assessed on January 2020).
46 C. Hansch, A. Leo and D. H. Hoekman, *Exploring QSAR.: Hydrophobic, Electronic and Steric Constants*, ACS Professional reference Books, Washington USA, 1995.
47 See for instance: (a) I. Hussain and A. Ali, *J. Phytochemistry Biochem*., 2017, **1**, 1000104; (b) V. Angelova, V. Karabeliov, P. A. Andreeva-Gateva and J. Tchekalarova, *Drug Dev. Res*., 2016, **77**, 379-392; (c) G. Verma, A. Marella, M. Shaquiquzzaman, M. Akhtar, M. R. Ali, and M. M. Alam, *J Pharm. Bioallied Sci.*, 2014, **6**, 69–80.
48 Selected reviews on hydrazine derivatives in medicinal chemistry: (a) Ł. Popiołek, *Med. Chem. Res*., 2017, **26**, 287-301; (b) N. Singh, R. Ranjana, M. Kumari, and B. Kumar, *Int. J. Pharm. Clin. Res*., 2016, **8**, 162–166.
49 (a) D.-C. Wei, Y. Pan, H. Wang, W.-J Xu, C. Chen, J.-H. Zheng and D. Cai, *Eur. Rev. Med. Pharmacol. Sci.*, 2018, **22**, 4720–4729; (b) M. Hayakawa, K. Kawaguchi, H. Kaizawa, T. Koizumi, T. Ohishi, M. Yamano, M. Okada, M. Ohta, S. Tsukamoto, F. I. Raynaud, P. Parker, P. Workman and M. D. Waterfield, *Bioorg Med Chem*., 2007, **15**, 5837–5844.
50 A. R. Salian, S. Foro and B. T. Gowda, *Acta Cryst. Sect. E.* 2018, **74**, 1613–1618.
51 D. Barton and W.D. Ollis (eds.), Comprehensive Organic Chemistry, Pergamon, Oxford, U. K., 1979.
52 A. Weissberger, B. W. Rossiter and J. F. Hamilton, *Physical Methods of Chemistry. Electrochemical Methods*, ed. Wiley-interscience: New York, USA, 1986; Vol. 4, Chapter 4.
53 D. R. Laws, J. Sheats, A. L. Rheingold and W. E. Geiger, *Langmuir*, 2010, **26**, 15010-15021.
54 J. Zhang, B. Yang, Y. Yang and B. Zhang, *Front. Chem. China*, 2009, **4**, 52–57.
55 Y. Shao, Z. Gan, E. Epifanovsky, , A. T. B. Gilbert, M. Wormit, J. Kussmann, A. W. Lange, A. Behn, J. Deng, X. Feng, D. Ghosh, M. Goldey, P. R. Horn, L. D. Jacobson, I. Kaliman, R. Z. Khaliullin, T. Kuś, A. Landau, J. Liu, E. I. Proynov, Y. M. Rhee, R. M. Richard, M. A. Rohrdanz, R. P. Steele, E. J. Sundstrom, H. L. Woodcock III, P. M. Zimmerman, D. Zuev, B. Albrecht, E. Alguire, B. Austin , G. J. O. Beran, Y. A. Bernard, E. Berquist , K. Brandhorst, K. B. Bravaya, S. T. Brown, D. Casanova, C-M. Chang, Y. Chen, S. H. Chien, K. D. Closser, D. L. Crittenden, M. Diedenhofen, R. A. DiStasio jr., H. Do, A. D. Dutoi, R. G. Edgar, S. Fatehi, L. Fusti-Molnar, A. Ghysels, A. Golubeva-Zadorozhnaya, J. Gomes, M. W. D. Hanson-Heine, P. H. P. Harbach, A. W. Hauser, E. G. Hohenstein, Z. C. Holden, T-C. Jagau, H. Ji, B. Kaduk, K. Khistyaev, J. Kim, J. Kim, R. A. King, P. Klunzinger, D. Kosenkov, T. Kowalczyk, C. M. Krauter, K. U. Lao, A. D. Laurent, K. V. Lawler, S. V. Levchenko, C. Y. Lin, F. Liu, E. Livshits, R. C. Lochan, A. Luenser, P. Manohar, S. F. Manzer, S.-Ping Mao, N. Mardirossian, A. V. Marenich, S. A. Maurer, N. J. Mayhall, E. Neuscamman, C. M. Oana, R. Olivares-Amaya, D. P. O'Neill, J. A. Parkhill, T. M. Perrine, R. Peverati, A. Prociuk, D. R. Rehn, E. Rosta, N. J. Russ, S. M. Sharada, S. Sharma, D. W. Small, A. Sodt, T. Stein, D. Stuck, Y-C. Su, A. J. W. Thom, T. Tsuchimochi, V. Vanovschi, L. Vogt, O. Vydrov, T. Wang, M. A. Watson, J. Wenzel , A. White, C. F. Williams, J. Yang, S. Yeganeh, S. R. Yost, Z-Q.You, I. Y. Zhang, X. Zhang, Y. Zhao, B. R. Brooks, G. K. L. Chan, D. M. Chipman, C. J. Cramer, W. A. Goddard III, M. S. Gordon, W. J. Hehre, A. Klamt, H. F. Schaefer III, M. W. Schmidt, C. D. Sherrill, D. G. Truhlar, A. Warshel, X. Xu, A. Aspuru-Guzik, R. Baer, A. T. Bell, N. A. Besley, J-D. Chai, A. Dreuw, B. D. Dunietz, T. R. Furlani, S. R. Gwaltney, C-P. Hsu, Y. Jung, J. Kong, D. S. Lambrecht, W. Liang, C. Ochsenfeld, V. A. Rassolov, L. V. Slipchenko, J. E. Subotnik, T. Van Voorhis, J. M. Herbert, A. I. Krylov, P. M. W. Gill and M. Head-Gordon, *Mol. Phys.* 2015, **113**, 184–215.
56 *Spartan 18, v. 1.3.0.* Wavefunction, Irvine (CA), 2019.
57 (a) A. D. Becke, *J. Chem. Phys.* 1993, **98**, 5648–5652; (b) C. Lee, W. Yang and R. G. Parr, *Phys. Rev. B*, 1988, **37**, 785–789.
58 (a) S. K. Yeo and J-L. Guan, *Trends Cancer*, *2017*, **3**, 753–760; (b) X. Dai, H. Cheng, Z. Bai and J. Li, *J. Cancer*., 2017, **8**, 3131–3141; (c) K. Dias, A. Dvorkin-Gheva, R. M. Hallett, Y. Wu, J. Hassell, G. R. Pond, M. Levine, T. Whelan and A. L. Bane, *PLoS One*., 2017, 12, e0168669.
59 (a) J. M. Heldt, N. Fischer-Durand, M. Salmain, A. Vessières and G. Jaouen, *J. Organomet. Chem.,* 2004, **689**, 4775–4782; (b) M. Hromadová, M. Salmain, R. Sokolová, L. Pospísil and G. Jaouen, *J. Organomet. Chem.,* 2003, **668**, 17 –24.
60 D. D. Perrin and W. L. F. Amarego, *Purification of Laboratory Chemicals*, Butterworth–Heinemann, Oxford, UK, 4th ed, 1996.
61 Bruker Analytical X-ray Systems (2006, June) Apex2, Version 2 User Manual, M86-E01078, Madison, WI, USA.
62 L. Palatinus and G. Chapuis, *J. Appl. Cryst*., 2007, **40** 786–790.
63 P. W. Betteridge, J. R. Carruthers, R. I. Cooper, K. Prout and D. J. Watkin, *J. Appl. Cryst*., 2003, **36**, 1487.
64 P. C. Hariharan and J. A. Pople, *Theor. Chim. Acta* 1973, **28**, 213–222.
65 M. M. Francl, W. J. Pietro, W. J. Hehre, J. S. Binkley, M. S. Gordon, D. J. DeFrees and J. A. Pople, *J. Chem. Phys*. 1982, **77**, 3654–3665.
66 V. A. Rassolov, J. A. Pople, M. A. Ratner and T. L. Windus*, J. Chem. Phys.* 1998, **109**, 1223–1229.
67 P. J. Hay and W. R. Wadt, *J. Chem. Phys*., 1985, **82**, 270–283.
68 T. A. Halgren, *J. Comp. Chem*., 1996, **17**, 490–519.
69 K. T. Givens, S. Kitada, A. K. Chen, J. Rothschiller and D. A. Lee, *Invest. Ophthalmol. Visual Sci*., 1990, **31**, 1856– 1862.
70 J. Li, K. Shi, Z. F. Sabet, W. Fu, H. Zhou, S. Xu, T. Liu, M. You, M. Cao, M. Xu, X. Cui, B. Hu, Y. Liu and C. Chen, *Sci. Adv.,* 2019, **5**, eaax0937.

View Article Online
DOI: 10.1039/D0DT01756F

Table of contents graphic and Sinopsis

Novel Homo- (Fe_2) and Heterobimetallic [(Fe,M) with M = Re or Mn] Sulfonyl Hydrazones

.

Yosselin Huentupil,[a] Patricio Chung,[a] Néstor Novoa,[a] Rodrigo Arancibia,*[a] Pascal Roussel,[b] Juan Oyarzo,[c] A. Hugo Klahn,[c] Carlos P. Silva,[d] Carme Calvis,[e] Ramon Messeguer,[e] Ramón Bosque,[f] Concepción López *[f]

The novel ferrocenyl sulfonyl hydrazide (**2**) and its homo (**4**) and heterobimetallic (**5a** and **5b**) imines were prepared and characterized. A comparative study of their electrochemical, spectroscopic and antitumoral properties is also described.